Mechanical and thermal couplings in helical strands

Dansong Zhang, Martin Ostoja-Starzewski, Loïc Le Marrec

Mechanical and thermal couplings in helical strands

Dansong Zhang[a], Martin Ostoja-Starzewski[b], and Loïc Le Marrec[c]

[a]Department of Mechanical Science & Engineering, University of Illinois at Urbana–Champaign, Urbana, IL, USA; [b]Department of Mechanical Science & Engineering, Institute for Condensed Matter Theory and Beckman Institute, University of Illinois at Urbana-Champaign, Urbana, IL, USA; [c]Université de Rennes, IRMAR – UMR 6625, Rennes, France

A generalized Timoshenko rod model is developed for helical strands and helically reinforced cylinders. The thermomechanical constitutive law has five effective elastic moduli, and two thermal coefficients, which can be obtained with the finite element method, or partly from analytic solutions. The model predicts nonclassical bending and thermoelastic behavior of helical strands. First, bending–shearing coupling is explicitly captured, which leads to non-planar bending under a transverse shear force, or a bending moment. Second, torsion and thermal expansion are coupled due to structural chirality. The dispersion relation of harmonic thermoelastic waves is governed by four non-dimensional parameters: two thermoelastic coupling constants, one chirality parameter and the Fourier number. The quasi-longitudinal and the quasi-torsional waves ("quasi" meaning the longitudinal mode is always coupled with a small torsional motion, and vice versa, due to chirality) are dispersive and damped, and dependent on tem-perature. The adiabatic-isothermal transition of the wave propagation is determined by the Fourier number.

Introduction

Helical strands, or helically wound cables, are made of layers of individual wires helically wrapped around a common central axis. They are commonly seen in ropes and power transmission cables. The helical wrapping introduces mirror asymmetry, or chirality into the structure, leading to effective properties not present in the base material. Under the no-slip condition, helical strands are in close analogy to helical-fiber-reinforced composites [1].

A critical part of modeling helical strands is to find their effective properties which are functions of the strand configuration, the material parameters, and the interfacial conditions. It can be done by either modeling the wires individually, or by effectively treating the helical layers as concentric helically reinforced cylinders. The second approach replaces each layer of wires with an effective continuum, and is termed the "semi-continuous" method in the literature [2].

One most prominent effect of chirality in helical strands is the coupling between tension and torsion, i.e., an axial tensile load induces a twist, and an axial torque induces an extension. This effect has been widely studied in the literature [3,4]. Transverse deformations of the strand can also be incorporated by adding a bending stiffness into the overall constitutive law [5,6]. Given the stiffnesses, the model essentially reduces the whole strand to an effective Euler–Bernoulli rod.

CONTACT Martin Ostoja-Starzewski martinos@illinois.edu Department of Mechanical Science & Engineering Institute, for Condensed Matter Theory and Beckman Institute, University of Illinois at Urbana-Champaign, Urbana, IL 61801, USA.

However, there are cases when this model is not sufficient to explain all the chiral effects in helical strands. Crossley solved the flexural problems of helically reinforced cylinders based on 3 D elasticity, and discovered that an extra bending moment is required to make sure the bending is planar [7,8]. This is another phenomenon caused by the chirality of the strands. However, as is shown in the current article, the classical rod model fails to predict this behavior and a generalization of the model is required.

Thermal–mechanical couplings are reported in the literature for helices and helical strands. Pipes and Hubert [9] studied helical nanotube/polymer arrays by modeling them as concentric cylinders. The effective axial, circumferential, and shear coefficients of thermal expansion for carbon nanotube arrays are obtained as functions of the lay angle. Karathanasopolous *et al.* analytically derived the coefficients for the thermal effect on the axial, torsional, and radial loads on a single helix [10]. Ieşan [11,12] solved the deformation of isotropic chiral cylinders using the equilibrium theory of Cosserat thermoelastic continuum, and found that a temperature field produced torsional effects. Thus, to account for thermal effects, the rod model needs to be further extended.

The thermoelastic wave propagations in isotropic [13–15], transversely isotropic [16] and layered anisotropic [17] media were solved with the theory of thermoelasticity [18,19]. It was found that the phase velocities of the waves are modified due to the thermal effects and material anisotropy. Tomar and Khurana [20] solved time harmonic wave propagation in a thermoelastic chiral medium using micropolar thermoelasticity. Temperature field is added to the set of equations for hemitropic micropolar materials. All the waves are found to be dispersive and the coupled dilatational waves are attenuated and temperature dependent. The thermoelastic waves in helical strands have not been investigated except in one of our earlier articles [21], where it was assumed that there is no coupling between torsion and temperature fields.

A model that effectively reduces a helically reinforced beam or a helical strand to a rod was proposed in [22]. It is a generalized rod model, with a 6 by 6 stiffness matrix, taking into account the shear flexibility. In the current article, the rod model is restated, with a slightly more general representation. Thermal expansion is also introduced into the rod constitutive law. The derivation starts from the generalized Timoshenko rod model, with a full 6×6 mechanical stiffness matrix and six thermal coefficients. For a helical strand, the inherent structural symmetry results in many zero entries in the stiffness and thermal coefficients. The final form of the themo-mechanical constitutive law for a helical strand is then obtained, with five non-zero constants for mechanical deformation and two for thermal expansion. The procedures for estimating the values of the nonzero constants are stated. With the thermomechanical constitutive law, the general thermoelastic behavior of helical strands can be solved. In particular, two mechanical and thermal couplings in helical strands are investigated. First, the aforementioned nonclassical bending behavior is predicted. Second, the celerities (phase velocities) and dampings of thermoelastic waves in helical strands are solved, with discussions on the modifications of the wave solutions due to structural chirality and thermomechanics. Note that all the discussions are for helical strands with no internal slip at contacting surfaces, and hence, the discoveries of the chiral effects are equally applicable to helical-fiber-reinforced composites. It has been reported that the interfacial slipping condition has influence on the bending stiffness [23], but not on the tensile and torsional stiffnesses as tensile and torsional loads do not induce slip [6].

The article is organized as follows, the Timoshenko rod model accounting for only the mechanical behavior is stated and the procedure of estimating the effective moduli proposed. The nonclassical bending behavior is predicted by the model and also verified by a finite element analysis. In a second part, the model is extended to include thermal effects. First, the final form of the thermomechanical constitutive relation is established by introducing thermal expansion terms. Then, the thermoelastic wave equations are derived for helical strands. Finally, the effects of thermoelastic coupling on the harmonic wave solutions are detailed.

Elastic rod model for helical strands

Consider a helical strand with a length of L. A Cartesian frame $(O; \mathbf{e}_1, \mathbf{e}_2, \mathbf{e}_3)$ is defined. It is common in the literature that an effective rod model of a helical strand is expressed as [2,5,6,24]

$$\begin{Bmatrix} N_3 \\ M_3 \\ M_1 \\ M_2 \end{Bmatrix} = \begin{bmatrix} (EA) & k_{TR} & 0 & 0 \\ k_{RT} & (GJ) & 0 & 0 \\ 0 & 0 & (EI) & 0 \\ 0 & 0 & 0 & (EI) \end{bmatrix} \begin{Bmatrix} \gamma_3 \\ \kappa_3 \\ \kappa_1 \\ \kappa_2 \end{Bmatrix} \tag{1}$$

This formulation follows the Euler–Bernoulli beam framework, neglecting the shear rigidities of the cross section. Here (EA) is the effective tensile stiffness, (GJ) is the effective torsional stiffness, and (EI) is the effective bending stiffness, while $k_{TR} = k_{RT}$ characterizes the coupling between tension and torsion. We also have the deformation $\gamma_3 = \Delta u_3/\Delta L$ and $\kappa_i = \Delta\theta_i/\Delta L$ $(i = 1, 2, 3)$, with ΔL being the length of a segment along the axis of the strand. There are a lot of articles on accurately computing the effective stiffnesses in the formula. The readers can refer to a review of the models in [3,4]. Most models use a discrete approach that treats each wire individually as a curved thin rod and then assembles them based on deformation constraints [5,25–28]. In contrast, Raoof and Hobbs [29] and Jolicoeur and Cardou [6] proposed semicontinuous models that effectively homogenize each layer of helical wires as an orthotropic elastic cylinder. The effective stiffnesses in Eq. (1) are derived in terms of the elastic constants of the "effective" orthotropic material by solving the elasticity of a cylinder.

Instead of the models above, we seek a Timoshenko model that considers the transverse shear rigidities of the cross section. Following the generalized Timoshenko theory in [30,31], the most general form of the constitutive relation of a non-homogeneous, anisotropic beam can be written as follows:

$$\begin{Bmatrix} N_1 \\ N_2 \\ N_3 \\ M_1 \\ M_2 \\ M_3 \end{Bmatrix} = \begin{bmatrix} C_{11} & C_{12} & C_{13} & C_{14} & C_{15} & C_{16} \\ C_{21} & C_{22} & C_{23} & C_{24} & C_{25} & C_{26} \\ C_{31} & C_{32} & C_{33} & C_{34} & C_{35} & C_{36} \\ C_{41} & C_{42} & C_{43} & C_{44} & C_{45} & C_{46} \\ C_{51} & C_{52} & C_{53} & C_{54} & C_{55} & C_{56} \\ C_{61} & C_{62} & C_{63} & C_{64} & C_{65} & C_{66} \end{bmatrix} \begin{Bmatrix} \gamma_1 \\ \gamma_2 \\ \gamma_3 \\ \kappa_1 \\ \kappa_2 \\ \kappa_3 \end{Bmatrix} \tag{2}$$

where γ_1 and γ_2 are the engineering shear strains.

Symmetry of rod constitutive behavior

For a specific rod geometry, many entries in the stiffness matrix $\mathbf{C}$ are zeros due to symmetry. While it is difficult to get the actual values of the nonzero entries for a helical strand (which will be discussed later), one can readily see how many such entries are present in the stiffness matrix $\mathbf{C}$ by assuming a helical strand possesses the same symmetries as a helically reinforced cylinder. To that end, we start from the Spencer constitutive law [32] of a transversely isotropic, linear elastic continuum with fiber orientation $\boldsymbol{\tau}$. The strain energy is

$$\Phi(\boldsymbol{\varepsilon}, \boldsymbol{\tau}) = \frac{\lambda}{2}(\mathrm{Tr}(\boldsymbol{\varepsilon}))^2 + \mu \mathrm{Tr}(\boldsymbol{\varepsilon}^2) + \alpha_1 \mathrm{Tr}(\boldsymbol{\Sigma}\boldsymbol{\varepsilon})\mathrm{Tr}(\boldsymbol{\varepsilon}) + \frac{\alpha_2}{2}(\mathrm{Tr}(\boldsymbol{\Sigma}\boldsymbol{\varepsilon}))^2 + \alpha_3 \mathrm{Tr}(\boldsymbol{\Sigma}\boldsymbol{\varepsilon}^2) \tag{3}$$

where $\boldsymbol{\Sigma} = \boldsymbol{\tau} \otimes \boldsymbol{\tau}$ is the orientation tensor, and

$$\boldsymbol{\tau} = \sin\beta(-\sin\varphi \mathbf{e}_1 + \cos\varphi \mathbf{e}_2) + \cos\beta \mathbf{e}_3 \tag{4}$$

given β the local lay angle and φ the azimuthal coordinate in the cylindrical coordinate system (r, φ, z) oriented along $\mathbf{e}_3 \equiv \mathbf{e}_z$. The stress then becomes:

$$\boldsymbol{\sigma} = \lambda \mathrm{Tr}(\boldsymbol{\varepsilon})\mathbb{I} + 2\mu\boldsymbol{\varepsilon} + \alpha_1\left[\mathrm{Tr}(\boldsymbol{\Sigma}\boldsymbol{\varepsilon})\mathbb{I} + \mathrm{Tr}(\boldsymbol{\varepsilon})\boldsymbol{\Sigma}\right] + \alpha_2 \mathrm{Tr}(\boldsymbol{\Sigma}\boldsymbol{\varepsilon})\boldsymbol{\Sigma} + \alpha_3(\boldsymbol{\Sigma}\boldsymbol{\varepsilon} + \boldsymbol{\varepsilon}\boldsymbol{\Sigma}) \tag{5}$$

where $\mathbb{I}$ is the identity tensor, or in indicial notation,

$$\sigma_{ij} = \lambda\varepsilon_{kk}\delta_{ij} + 2\mu\varepsilon_{ij} + \alpha_1\left(\tau_k\tau_l\varepsilon_{kl}\delta_{ij} + \tau_i\tau_j\varepsilon_{kk}\right) + \alpha_2\tau_i\tau_j\tau_k\tau_l\varepsilon_{kl} + \alpha_3\left(\tau_i\tau_k\varepsilon_{kj} + \tau_j\tau_k\varepsilon_{ki}\right) \tag{6}$$

The parameters in Eq. (3) are related to the five independent elastic moduli E_T, E_L, G_L, G_T, ν_L, for a transversely isotropic material. E_T and E_L are the elastic moduli in the transverse and the longitudinal directions of the helical fibers, respectively. G_L is the shear modulus for shear strains between the longitudinal direction and any transverse direction, G_T is the shear modulus in the transverse plane, while ν_L is Poisson's ratio for strain in the longitudinal direction caused by stress in any transverse direction. In particular, $\alpha_3 = 2(G_\mathrm{L} - G_\mathrm{T})$ and $\mu = G_\mathrm{T}$ [24].

We then impose the Timoshenko beam assumption, i.e., for any point P on the cross section $\mathcal{S}$, with a position vector $\overrightarrow{O'P} = x_1\mathbf{e}_1 + x_2\mathbf{e}_2$, the displacement $\mathbf{w}$ of P is controlled by the displacement $\mathbf{u}$ of the center of mass O' and the rotation vector $\boldsymbol{\theta}$ of the rigid section:

$$\mathbf{w} = \mathbf{u} + \boldsymbol{\theta} \times \overrightarrow{O'P} \tag{7}$$

Here, $\mathbf{w} = w_j(x_1, x_2, x_3, t)\mathbf{e_j}, \mathbf{u} = u_j(x_3, t)\mathbf{e_j}$, and $\boldsymbol{\theta} = \theta_j(x_3, t)\mathbf{e_j}$, where Einstein's summation convention is used. The deformation gradient is [33]

$$\nabla\mathbf{w} = \frac{\partial\mathbf{w}}{\partial x_1} \otimes \mathbf{e}_1 + \frac{\partial\mathbf{w}}{\partial x_2} \otimes \mathbf{e}_2 + \frac{\partial\mathbf{w}}{\partial x_3} \otimes \mathbf{e}_3$$

with

$$\frac{\partial\mathbf{w}}{\partial x_1} = \boldsymbol{\theta} \times \mathbf{e}_1, \qquad \frac{\partial\mathbf{w}}{\partial x_2} = \boldsymbol{\theta} \times \mathbf{e}_2, \qquad \frac{\partial\mathbf{w}}{\partial x_3} = \frac{\partial\mathbf{u}}{\partial x_3} + \frac{\partial\boldsymbol{\theta}}{\partial x_3} \times \overrightarrow{O'P}$$

The small strain tensor $\boldsymbol{\varepsilon} = \frac{1}{2}(\nabla\mathbf{w} + (\nabla\mathbf{w})^\mathrm{T})$ is then obtained explicitly as follows:

$$\boldsymbol{\varepsilon} = \begin{pmatrix} 0 & 0 & \frac{1}{2}\left(u_1' - \theta_2 - x_2\theta_3'\right) \\ 0 & 0 & \frac{1}{2}\left(u_2' + \theta_1 + x_1\theta_3'\right) \\ \frac{1}{2}\left(u_1' - \theta_2 - x_2\theta_3'\right) & \frac{1}{2}\left(u_2' + \theta_1 + x_1\theta_3'\right) & u_3' + x_2\theta_1' - x_1\theta_2' \end{pmatrix}$$

where we use prime for $\partial/\partial x_3$. The force $\mathbf{N} = N_i\mathbf{e_i}$ and moment $\mathbf{M} = M_i\mathbf{e_i}$ on a cross section are then obtained by the following integration:

$$\mathbf{N} = \int_\mathcal{S} \boldsymbol{f}\ \mathrm{d}x_1\mathrm{d}x_2, \qquad \mathbf{M} = \int_\mathcal{S} \overrightarrow{O'P} \times \boldsymbol{f}\ \mathrm{d}x_1\mathrm{d}x_2 \tag{8}$$

with $\boldsymbol{f} = \sigma_{j3}\mathbf{e_j}$ being the traction on an arbitrary point of the cross section.

Example I: Solid circular cylinder with uniform lay angle β

With the stress components given, the integration in Eq. (8) can be performed to obtain a constitutive relation in the form of Eq. (2) with the stiffness matrix

$$\mathbf{C} = \begin{bmatrix} \pi R^2 G_s & 0 & 0 & -\frac{\pi R^3}{2}C_f & 0 & 0 \\ 0 & \pi R^2 G_s & 0 & 0 & -\frac{\pi R^3}{2}C_f & 0 \\ 0 & 0 & \pi R^2 E & 0 & 0 & \pi R^3 C_f \\ -\frac{\pi R^3}{2}C_f & 0 & 0 & \frac{\pi R^4}{4}E & 0 & 0 \\ 0 & -\frac{\pi R^3}{2}C_f & 0 & 0 & \frac{\pi R^4}{4}E & 0 \\ 0 & 0 & \pi R^3 C_f & 0 & 0 & \frac{\pi R^4}{2}G_r \end{bmatrix} \tag{9}$$

where

$$\begin{aligned} E &= \lambda + 2\mu + \cos^2\beta\left(2\alpha_1 + 2\alpha_3 + \alpha_2\cos^2\beta\right) \\ G_s &= \mu + \frac{1}{8}\left[\alpha_2 \sin^2 2\beta + \alpha_3(3 + \cos 2\beta)\right] \\ G_r &= \mu + \frac{1}{8}\left[\alpha_2 \sin^2 2\beta + \alpha_3(3 + \cos 2\beta)\right] + \frac{\sin^2\beta}{4}\left(2\cos^2\beta\alpha_2 + \alpha_3\right) \\ C_f &= \frac{\sin 2\beta}{3}\left(\alpha_1 + \alpha_3 + \alpha_2\cos^2\beta\right) \end{aligned} \tag{10}$$

Here, E, G_s, G_r, and C_f are the effective moduli for extension, shear, torsion, and coupling, respectively. As pointed out in [22], when the lay angle is nonzero, the effective torsional modulus G_r is different than the effective transverse shear modulus G_s. Another observation is that C_f is nonzero when the lay angle is nonzero, i.e., there is coupling between tension and torsion, as well as between shearing and bending.

Example II: Solid circular cylinder with stepwise β

The lay angle β is a stepwise function of the radial position r:

$$\beta(r) = \begin{cases} 0, & r < r_0 \\ \beta, & r_0 < r < R \end{cases} \tag{11}$$

where R is the outer radius of the cable. This models a helical cable with one layer of helical wires and a straight core. Following the integration procedure mentioned above, we get $\mathbf{C}$ of the form

$$\mathbf{C} = \begin{bmatrix} \pi R^2 G_s & 0 & 0 & -\frac{\pi R^3}{2} C_f & 0 & 0 \\ 0 & \pi R^2 G_s & 0 & 0 & -\frac{\pi R^3}{2} C_f & 0 \\ 0 & 0 & \pi R^2 E_e & 0 & 0 & \pi R^3 C_f \\ -\frac{\pi R^3}{2} C_f & 0 & 0 & \frac{\pi R^4}{4} E_b & 0 & 0 \\ 0 & -\frac{\pi R^3}{2} C_f & 0 & 0 & \frac{\pi R^4}{4} E_b & 0 \\ 0 & 0 & \pi R^3 C_f & 0 & 0 & \frac{\pi R^4}{2} G_r \end{bmatrix} \tag{12}$$

where

$$G_s = \alpha_2\left(\frac{1}{16}\left(\xi^2 - 1\right)\cos(4\beta) - \frac{\xi^2}{16} + \frac{1}{16}\right) + \alpha_3\left(\frac{1}{8}\left(1 - \xi^2\right)\cos(2\beta) + \frac{\xi^2}{8} + \frac{3}{8}\right) + \mu \tag{13a}$$

$$C_f = -\frac{1}{6}\left(\xi^3 - 1\right)\sin(2\beta)(2\alpha_1 + \alpha_2\cos(2\beta) + \alpha_2 + 2\alpha_3) \tag{13b}$$

$$\begin{aligned} E_e = \alpha_1\Big(\left(1 - \xi^2\right)\cos(2\beta) + \xi^2 + 1\Big) + \alpha_2\Big(\frac{1}{2}\left(1 - \xi^2\right)\cos(2\beta) + \frac{1}{8}\left(1 - \xi^2\right)\cos(4\beta) + \frac{5\xi^2}{8} + \frac{3}{8}\Big) \\ + \alpha_3\Big(\left(1 - \xi^2\right)\cos(2\beta) + \xi^2 + 1\Big) + \lambda + 2\mu \end{aligned} \tag{13c}$$

$$\begin{aligned} E_b = \alpha_1\Big(-\left(\xi^4 - 1\right)\cos(2\beta) + \xi^4 + 1\Big) + \frac{1}{8}\alpha_2\Big(-4\left(\xi^4 - 1\right)\cos(2\beta) + \left(1 - \xi^4\right)\cos(4\beta) + 5\xi^4 + 3\Big) \\ + \alpha_3\Big(-\left(\xi^4 - 1\right)\cos(2\beta) + \xi^4 + 1\Big) + \lambda + 2\mu \end{aligned} \tag{13d}$$

$$G_r = \frac{1}{8}\left[\alpha_2\left(\xi^4 - 1\right)\cos(4\beta) - \alpha_2\xi^4 + \alpha_2 + 4\alpha_3\right] + \mu \tag{13e}$$

in which, $\xi = r_0/R$. Again, the effective torsional modulus G_r is different than the shear modulus G_s. However, in contrast to Eq. (9), the modulus of extension E_e and the modulus of bending E_b are also different here. In fact,

$$E_e - E_b = \frac{1}{2}\xi^2\left(1 - \xi^2\right)[4\alpha_1 + \alpha_2\cos(2\beta) + 3\alpha_2 + 4\alpha_3]\sin^2\beta \tag{14}$$

Note that $E_e = E_b$ when $\xi = 0$, i.e., when β is uniform.

Example III: Uniform pitch length

This is to model the case where we make a helical strand by clamping a bundle of fibers at one end, and twisting the other end. The strand obtained will have a uniform pitch length from the center to the edge of the cross section. With a small angle assumption, we have $\beta \approx kr$ where k is a constant. In this case, one can also get a stiffness matrix following the form of Eq. (12), with different stiffness values, i.e., $E_b \neq E_e$ and $G_s \neq G_r$ unless $\beta \equiv 0$.

From the above, the symmetry of a helical strand leads to a stiffness matrix of the form in Eq. (12). For a helically wound cable with a straight core, Example II is a better approximation, since we can treat the core as an inner region with $\beta = 0$, and the helices as an outer section with β constant. There are five independent effective moduli, E_e, G_s, E_b, G_r, and C_f, that are functions of the lay angle and the wires' diameters. However, the values of the effective moduli, do not follow Eq. (13), as the wires are separate from each other, and do not fill the annular space around the core. In addition, this form of stiffness matrix shows that the bending–shearing problem and the tension–torsion problem are uncoupled.

Procedure of estimating effective moduli

It is nontrivial to determine the values of the effective moduli in the rod models. In the semicontinuous model by Jolicoeur and Cardou, the elastic constants of the transversely isotropic cylinders can be estimated either by fitting results from thin rod models [24] or by modeling the contact between wires [2,6]. These authors also recommended the use of experimental data to achieve more reliable estimations [24].

For the Timoshenko model that we propose, we use the finite element analysis to estimate the effective moduli in Eq. (12) due to the following reasons. First, modeling the contact between wires with an analytic approach requires assumptions that are themselves to be verified. Second, finite element analysis for a helical strand is relatively quick and accurate. Third, the effective moduli do not depend on the length of the cable, and thus we can do the finite element analysis on a relatively short cable, the results from which can then be used for cables of arbitrary lengths.

Inferring the values of the effective moduli from finite element results requires solving an inverse problem. The forward problem is to solve the response of the cable under given boundary conditions. The equilibrium equations for the Timoshenko rod with no distributed loads are [22]

$$\begin{cases} \dfrac{\partial \mathbf{N}}{\partial x_3} = \rho A \dfrac{\partial^2 \mathbf{u}}{\partial t^2} \\ \dfrac{\partial \mathbf{M}}{\partial x_3} + \mathbf{e}_3 \times \mathbf{N} = \rho \mathbb{I}_{O'} \dfrac{\partial^2 \boldsymbol{\theta}}{\partial t^2} \end{cases} \tag{15}$$

which, for a static problem, have the following components in the Cartesian frame $(O; \mathbf{e}_1, \mathbf{e}_2, \mathbf{e}_3)$

$$N_1' = 0 \tag{16a}$$

$$N_2' = 0 \tag{16b}$$

$$N_3' = 0 \tag{16c}$$

$$M_1' - N_2 = 0 \tag{16d}$$

$$M_2' + N_1 = 0 \tag{16e}$$

$$M_3' = 0 \tag{16f}$$

With the constitutive relations obtained by the integration in Eq. (8), the equations of equilibrium can be solved for given boundary conditions.

For comparison, the constitutive equation for the Euler–Bernoulli beam model shown in Eq. (1), is re-written as

$$\begin{bmatrix} N_3 \\ M_1 \\ M_2 \\ M_3 \end{bmatrix} = [\mathbf{C}] \begin{bmatrix} u_3' \\ -u_2'' \\ u_1'' \\ \theta_3' \end{bmatrix} \tag{17}$$

with

$$[\mathbf{C}] = \begin{bmatrix} \pi R^2 E_{\mathrm{e}} & 0 & 0 & \pi R^3 C_f \\ 0 & \dfrac{\pi R^4}{4} E_{\mathrm{b}} & 0 & 0 \\ 0 & 0 & \dfrac{\pi R^4}{4} E_{\mathrm{b}} & 0 \\ \pi R^3 C_f & 0 & 0 & \dfrac{\pi R^4}{2} G_{\mathrm{r}} \end{bmatrix} \tag{18}$$

In Eq. (17), $\theta_1 = -u_2'$ and $\theta_2 = u_1'$ have been used, which are based on the assumption that there is no transverse shear strain in the cross section. N_3, M_1, M_2, and M_3 can be solved under given boundary conditions from Eq. (16). Then, N_1 and N_2 can be inferred using Eqs. (16d) and (16e).

Alternatively, there are many analytic models that give predictions of the effective moduli E_{e}, E_{b}, G_{r}, and C_f [5,25,26,34,35]. The values of G_{s}, however, are not available in the literature, since the analytic models follow the Euler–Bernoulli framework as in Eq. (1).

Numerical example of solving effective moduli

We consider a $1+6$ helical strand, made of a straight cylindrical core and six helical wires. The wires are perfectly bonded to the core, and there is no contact between neighboring wires. The radius of the core is $r_0 = 1.97$ mm, and the radius of the wires is $r_1 = 1.865$ mm, making the outer radius of the strand $R = 5.7$mm. The wires are made of a material with a Young's modulus $E_0 = 188$GPa and a Poisson's ratio $\nu = 0.3$. Helical strands of different lay angles of up to 17° are created and meshed. The strands have the same length 80 mm. It is verified that the effect of length on the results is minimal. For each strand, the mesh of the wires and the mesh of the core are stitched together with the procedure used in [23], and there is no contact between neighboring helical wires. The left ends of the cables are clamped. Several different types of boundary conditions are applied to the right end. Analytic solutions for each of the resulting boundary value problems (BVPs) are obtained by solving the equilibrium given by Eq. (16) with a stiffness matrix given by Eq. (12).

1. $u_3(L) = \delta$ and all other degrees of freedom are 0. The analytic solutions of the nonzero cross section forces and moments at $x_3 = L$ are

$$\frac{N_3}{\delta} = \frac{\pi R^2 E_e}{L} \tag{19a}$$

$$\frac{M_3}{\delta} = \frac{\pi R^3 C_f}{L} \tag{19b}$$

2. $\theta_3(L) = \theta$ and all other degrees of freedom are 0. The analytic solutions of the nonzero cross section forces and moments at $x_3 = L$ are

$$\frac{N_3}{\theta} = \frac{\pi R^3 C_f}{L} \tag{20a}$$

$$\frac{M_3}{\theta} = \frac{\pi R^4 G_r}{2L} \tag{20b}$$

3. $u_2(L) = \delta$ and all other degrees of freedom are 0. The analytic solutions of the nonzero cross section forces and moments at $x_3 = L$ are

$$\frac{N_2}{\delta} = \frac{3\pi G_s R^4 \left(E_b G_s - C_f^2\right)}{L\left(-3C_f^2 R^2 + 3E_b G_s R^2 + G_s^2 L^2\right)} \tag{21a}$$

$$\frac{M_2}{\delta} = \frac{3\pi C_f R^5 \left(C_f^2 - E_b G_s\right)}{2L\left(-3C_f^2 R^2 + 3E_b G_s R^2 + G_s^2 L^2\right)} \tag{21b}$$

$$\frac{M_1}{\delta} = \frac{3\pi G_s R^4 \left(E_b G_s - C_f^2\right)}{-6C_f^2 R^2 + 6E_b G_s R^2 + 2G_s^2 L^2} \tag{21c}$$

With the values of the left-hand side obtained from finite element simulations, each of the equations above gives one relation between the elastic constants. Some of these equations are linearly dependent, e.g., Eq. (19b) and Eq. (20a) are the same, Eqs. (21c) and (21a) are proportional. Therefore, we end up with five independent equations, Eqs. (19a),(19b),(20b),(21a), and (21b). The five unknowns E_e, C_f, G_s, E_b and G_r, can then be solved and written explicitly as functions of the loads:

$$E_e = (N_3/\delta) \cdot \frac{L}{\pi R^2} \tag{22a}$$

$$C_f = (M_3/\delta) \cdot \frac{L}{\pi R^3} \tag{22b}$$

$$G_r = (M_3/\theta) \cdot \frac{2L}{\pi R^4} \tag{22c}$$

$$G_s = -\frac{(N_2/\delta) \cdot (M_3/\delta) \cdot \frac{L}{2\pi R^2}}{(M_2/\delta)} \tag{22d}$$

$$E_b = \frac{L^3 (M_3/\delta)(N_2/\delta)^2 - 6L(M_2/\delta)(M_3/\delta)[2(M_2/\delta) + (M_3/\delta)]}{3\pi (N_2/\delta) R^4 [2(M_2/\delta) + (M_3/\delta)]} \tag{22e}$$

When the lay angle $\beta = 0$, it is known a priori that $C_f = 0$, and (M_2/δ) and (M_3/δ) are also approximately zero. Therefore, Eq. (22d) and (22e) can no longer be used to compute G_s and E_b. In fact, when $\beta = 0$, there are only three nontrivial independent equations Eqs. (19a),(20b), and (21a), leaving G_s and E_b undetermined. But we can still get G_s and E_b at zero lay angle by extrapolating their values at nonzero lay angles. It is noteworthy to emphasize that these BVPs are not arbitrarily chosen. They cover the three basic deformation modes, extension, torsion and bending. More importantly, one has to make sure the final set of equations for solving the elastic moduli are insensitive to small perturbations to the finite element results for the cross section loads,

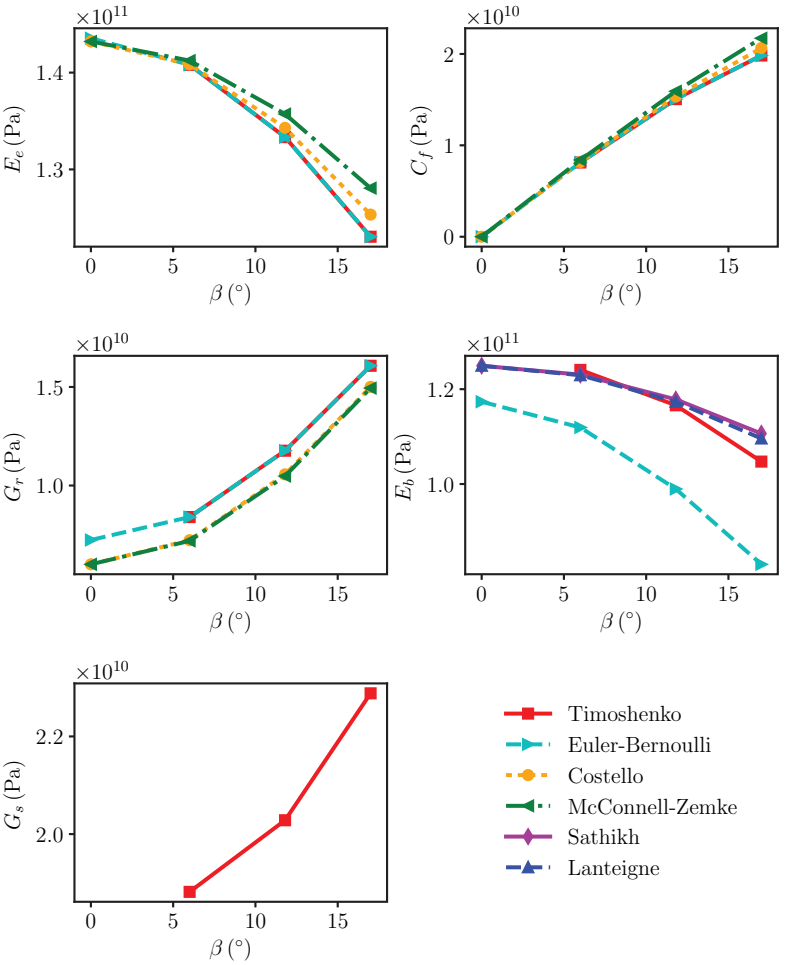

Figure 1. The values of the effective moduli i) for the Timoshenko model, ii) for the Euler-Bernoulli model, and iii) from analytic models in the literature (Costello, McConnell-Zemke, Sathikh, Lanteigne).

especially for the equations of G_s and E_b, which are likely nonlinear functions of the cross section loads. One can easily pick a set of BVPs such that the resultant equations are unstable to perturbations. Here, we have verified that Eq. (22) is well behaved in that sense.

As a comparison, the elastic moduli in the Euler–Bernoulli model can also be estimated with the finite element analysis. The analytic solutions for the cross section forces and moments under BVPs 1–3 are listed below.

1.
$$\frac{N_3}{\delta} = \frac{\pi R^2 E_e}{L} \tag{23a}$$
$$\frac{M_3}{\delta} = \frac{\pi R^3 C_f}{L} \tag{23b}$$

2.
$$\frac{N_3}{\theta} = \frac{\pi R^3 C_f}{L} \tag{24a}$$
$$\frac{M_3}{\theta} = \frac{\pi R^4 G_r}{2L} \tag{24b}$$

3.

$$\frac{N_2}{\delta} = \frac{3\pi R^4 E_b}{L^3} \tag{25a}$$

$$M_2 = 0 \tag{25b}$$

$$\frac{M_1}{\delta} = \frac{3\pi R^4 E_b}{2L^2} \tag{25c}$$

There are four effective moduli, E_e, E_b, C_f and G_r, and four independent equations: Eqs. (23a),(23b),(24b) and (25c). All the equations are uncoupled and linear, and are thus apparently well conditioned. Since Eqs. (23a),(23b) and (24b) are the same as Eqs. (19a),(19b) and (20b), respectively, the values of E_e, C_f, and G_r are identical to those for the Timoshenko model. Only E_b is, in general, different.

The values of the five moduli from the finite element analysis are shown in Figure 1. Alternatively, estimates of E_e, C_f, and G_r can also be obtained from analytic models under tension–torsion loads in the literature, e.g., the model by Costello [25], and the model by McConnell and Zemke [35]. E_b is proportional to the bending stiffness of the cable and it depends on the contact condition at the wire–core interfaces [3]. In this study, the wires are assumed to be perfectly bonded to the core. The corresponding bending stiffness can be estimated using analytic models, such as the one by Lanteigne [5] or that by Sathikh et al. [26]. The values of E_e, C_f, and G_r from the Timoshenko model and from the Euler–Bernoulli model are identical, and they are close to those from the analytic models. The values of E_b for the Timoshenko model are also close to those from the analytic models. But the Euler–Bernoulli model requires significantly lower E_b's to match the loads predicted by the finite element method. The reason for the lower E_b is because under BVP3, there is transverse shear strain in the cable, therefore, the Euler–Bernoulli beam assumption that the cross section remains orthogonal to the centerline is no longer valid, i.e., the Euler–Bernoulli model would overestimate the bending loads, if using the same effective bending moduli E_b. No report on analytic estimates of the effective shear modulus G_s has been seen in the literature. The shear correction factor κ for conventional Timoshenko beam model is implicitly incorporated into the effective shear moduli G_s here. G_s and G_r (in Figure 1) both increase with the lay angle, but G_s is greater than G_r.

Bending–shearing coupling in helical strands

Comparing Eq. (21) with Eq. (25), we see that the most significant difference is that the Timoshenko model predicts a nonzero M_2 when the beam is flexed by a displacement u_2, whereas the Euler–Bernoulli model predicts M_2 to be zero. According to Eqs. (21b) and (21c),

$$\frac{M_2}{M_1} = \frac{-C_f R}{G_s L} \tag{26}$$

Therefore, $M_2 = 0$ only when the coupling modulus $C_f = 0$, which corresponds to the case of a zero lay angle. M_2/M_1 is also proportional to R/L, suggesting the coupling effect is more significant for thick strands. The bending is also not planar, as

$$u_1 = -\frac{3C_f G_s R\left(Lx_3 - x_3^2\right)\delta}{L\left(-3C_f^2 R^2 + 3E_b G_s R^2 + G_s^2 L^2\right)} \tag{27}$$

which is non-zero unless $x_3 = 0$, or L. As a "conjugate," the case where the right end of the strand is subjected to a bending angle $\theta_2(L) = \theta$ is studied. Moreover, we add two more cases where the displacement and bending angle are applied in the 1-direction, i.e., we solve the following three BVP's:

4. $\theta_2(L) = \theta$ and all other degrees of freedom are 0.

Table 1. Cross section forces and moments predicted by different methods for $\beta = 0$.

Force or moment	FEA	Euler–Bernoulli
BVP4 N_1(N)	−7151	−7151
BVP4 N_2(N)	0.01786	0
BVP4 M_2(Nm)	389.2	381.4
BVP5 N_1(N)	1788	1788
BVP5 M_1(Nm)	−0.0001719	0
BVP5 M_2(Nm)	−71.51	−71.51
BVP6 N_1(N)	−0.01719	0
BVP6 N_2(N)	7151	7151
BVP6 M_1(Nm)	389.2	381.4

There are no predictions from the Timoshenko model because when $\beta = 0$, Eqs. (22d) and (22e) are no longer valid.

5. $u_1(L) = \delta$ and all other degrees of freedom are 0.
6. $\theta_1(L) = \theta$ and all other degrees of freedom are 0.

Since all the effective moduli are known for the Timoshenko and the Euler–Bernoulli models, The cross section loads for BVP4-BVP6 can be readily solved using these models. For BVP4, the Timoshenko model gives

$$\frac{N_2}{\theta} = \frac{3\pi C_f R^5\left(C_f^2 - E_b G_s\right)}{2L\left(-3C_f^2R^2 + 3E_bG_sR^2 + G_s^2L^2\right)} \tag{28a}$$

$$\frac{M_2}{\theta} = -\frac{\pi R^4\left(C_f^2 - E_bG_s\right)(3E_bR^2 + 4G_sL^2)}{4L\left(-3C_f^2R^2 + 3E_bG_sR^2 + G_s^2L^2\right)} \tag{28b}$$

$$\frac{N_1}{\theta} = \frac{3\pi G_s R^4\left(C_f^2 - E_bG_s\right)}{-6C_f^2R^2 + 6E_bG_sR^2 + 2G_s^2L^2} \tag{28c}$$

and the Euler–Bernoulli model gives

$$\frac{N_2}{\theta} = 0 \tag{29a}$$

$$\frac{M_2}{\theta} = \frac{\pi R^4 E_b}{L} \tag{29b}$$

$$\frac{N_1}{\theta} = -\frac{3\pi R^4 E_b}{2L^2} \tag{29c}$$

Again, the bending–shearing coupling leads to a non-zero N_2. Also, from Eqs. (28a) and (28c), we have

$$\frac{N_2}{N_1} = \frac{C_f R}{G_s L} \tag{30}$$

suggesting $N_2 = 0$ only when the lay angle $\beta = 0$, and the coupling is more significant for thick strands. The bending is also not planar, as the displacement u_2 is nonzero except at the left and right ends:

$$u_2 = -\frac{C_f G_s R\left(L^2x_3 - x_3^3\right)\theta}{L\left(-3C_f^2R^2 + 3E_bG_sR^2 + G_s^2L^2\right)} \tag{31}$$

The observations above also show that the bending deformations in the two cross-sectional principal directions are coupled, with the extent of coupling characterized by C_f, as is also demonstrated by the dynamic equations of motion in Ref. [22].

Table 2. Cross section forces and moments predicted by different methods for $\beta = 6^{\circ}$.

Force or moment	FEA	Timoshenko	Euler–Bernoulli
BVP4 N_1(N)	−2579	−2579	−2579
BVP4 N_2(N)	−28.12	−28.12	**0**
BVP4 M_2(Nm)	394.9	395.4	394.2
BVP5 N_1(N)	225	225	225
BVP5 M_1(Nm)	−0.2809	−0.2812	**0**
BVP5 M_2(Nm)	−25.79	−25.79	−25.79
BVP6 N_1(N)	−28.09	−28.12	**0**
BVP6 N_2(N)	2579	2579	2579
BVP6 M_1(Nm)	394.9	395.4	394.2

Values significantly different than FEA are made bold.

Table 3. Cross section forces and moments predicted by different methods for $\beta = 11.8^{\circ}$.

Force or moment	FEA	Timoshenko	Euler–Bernoulli
BVP4 N_1(N)	−4372	−4375	−4373
BVP4 N_2(N)	−162.5	−162.5	**0**
BVP4 M_2(Nm)	337.7	339.9	336.2
BVP5 N_1(N)	758.6	758.6	758.2
BVP5 M_1(Nm)	−1.623	−1.625	**0**
BVP5 M_2(Nm)	−43.72	−43.75	−43.73
BVP6 N_1(N)	−162.3	−162.5	**0**
BVP6 N_2(N)	4373	4375	4373
BVP6 M_1(Nm)	337.7	339.9	336.2

Values significantly different than FEA are made bold.

Table 4. Cross section forces and moments predicted by different methods for $\beta = 17^{\circ}$.

Force or Moment	FEA	Timoshenko	Euler–Bernoulli
BVP4 N_1(N)	−5327	−5327	−5328
BVP4 N_2(N)	−332.4	−332.4	**0**
BVP4 M_2(Nm)	281.1	284.9	280
BVP5 N_1(N)	1352	1352	1352
BVP5 M_1(Nm)	−3.322	−3.324	**0**
BVP5 M_2(Nm)	−53.27	−53.27	−53.28
BVP6 N_1(N)	−332.2	−332.4	**0**
BVP6 N_2(N)	5328	5327	5328
BVP6 M_1(Nm)	281.1	284.9	280

Values significantly different than FEA are made bold.

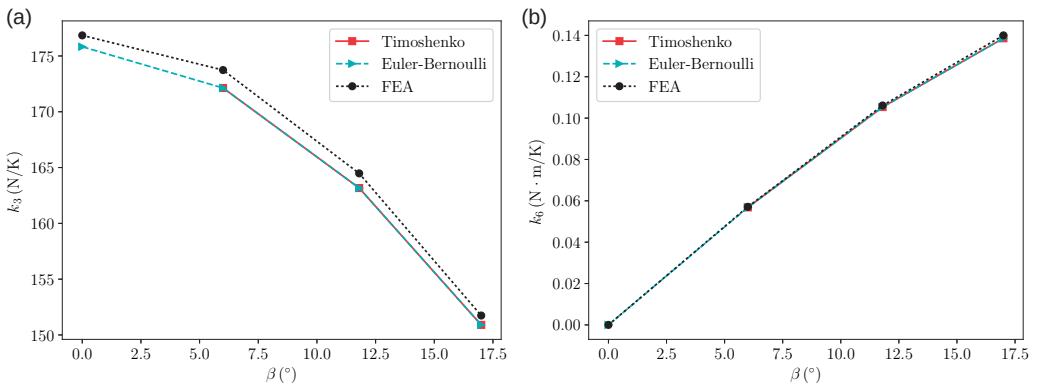

Figure 2. The thermal coefficients k_3 and k_6.

The solutions from the Timoshenko model are then verified by finite element analysis. Tables 1–4 show that with the Euler–Bernoulli model, N_2 for BVP4, M_1 for BVP5, and N_1 for BVP6 are always zero, because it neglects the coupling between shearing and bending. On the other hand, the Timoshenko model gives predictions very close to the finite element results for all cross section forces and moments. The fact that the model is equally good for displacement boundary conditions applied in both the 1- and 2-directions suggests that the strand is "quasi-isotropic" within the cross section.

Thermoelastic rod model for helical strands

Constitutive relation with thermal expansion

The effect of thermal expansion can be introduced into the constitutive law as an extra term:

$$\begin{Bmatrix} N_1 \\ N_2 \\ N_3 \\ M_1 \\ M_2 \\ M_3 \end{Bmatrix} = \begin{bmatrix} C_{11} & C_{12} & C_{13} & C_{14} & C_{15} & C_{16} \\ C_{21} & C_{22} & C_{23} & C_{24} & C_{25} & C_{26} \\ C_{31} & C_{32} & C_{33} & C_{34} & C_{35} & C_{36} \\ C_{41} & C_{42} & C_{43} & C_{44} & C_{45} & C_{46} \\ C_{51} & C_{52} & C_{53} & C_{54} & C_{55} & C_{56} \\ C_{61} & C_{62} & C_{63} & C_{64} & C_{65} & C_{66} \end{bmatrix} \begin{Bmatrix} \gamma_1 \\ \gamma_2 \\ \gamma_3 \\ \kappa_1 \\ \kappa_2 \\ \kappa_3 \end{Bmatrix} - \begin{Bmatrix} k_1 \\ k_2 \\ k_3 \\ k_4 \\ k_5 \\ k_6 \end{Bmatrix} \Theta \tag{32}$$

Analogous to the stiffness matrix $\mathbf{C}$, the thermal expansion coefficient vector $\{\mathbf{k}\}$ has zero entries depending on the underlying symmetry of the structure and the materials. In the case where the cable is made of a material with a uniform and isotropic coefficient of thermal expansion (CTE) η, a temperature increase Θ is equivalent to introducing a mechanical strain $\{\gamma_1 \quad \gamma_2 \quad \gamma_3 \quad \kappa_1 \quad \kappa_2 \quad \kappa_3\}^{\mathrm{T}} = \{0 \quad 0 \quad -\eta\Theta \quad 0 \quad 0 \quad 0\}^{\mathrm{T}}$, and thus $[\mathbf{C}]$ and $\{\mathbf{k}\}$ are related by

$$k_i = C_{i3}\eta, \quad i = 1...6 \tag{33}$$

In the case of a helical strand that follows Eq. (12):

$$k_3 = \pi R^2 E_e \eta, \quad k_6 = \pi R^3 C_f \eta, \quad \text{other } k_i = 0 \tag{34}$$

The same is true for Euler–Bernoulli models. Therefore, in this case, not only the zero entries in $\{\mathbf{k}\}$ are identified, but also the values of the nonzero k_i's are readily obtained from the mechanical stiffnesses E_e and C_f. Equation (34) shows that a uniform temperature increase leads to tensile and torsional loads, but has no effect on the bending moments and transverse shear forces. This equation can be verified with finite element analysis on the helical cables defined earlier. The CTE of the material is set to 1.2×10^{-5} K^{-1}. The strand is initially stress free, and then subjected to a uniform temperature increase of 100 K. The cross section loads are computed and used to infer k_i's. In the meantime, k_i's can be computed using Eq. (34), with the values of moduli already estimated above for the Timoshenko and the Euler–Bernoulli model, respectively. The values of k_3 and k_6 from the thermal finite element analysis compare very well with Eq. (34), as is shown in Figure 2. In the meantime, N_1 and N_2 remain around 0.01N, negligible compared with N_3 which is of the order of 10^4 N. M_1 and M_2 are also around 0.005 $\mathrm{N \cdot m^2}$, negligible compared with M_3 which is up to 14 $\mathrm{N \cdot m^2}$ for the largest lay angle.

In a more general case where the CTE is anisotropic, a simple relation between k_i and C_{ij} such as Eq. (34) does not exist, but one can still follow the procedure in the section "Symmetry of rod constitutive behavior" to identify the possible zero k_i's. Again, this is based on the assumption that the helical strand follows the same symmetry as a helically reinforced cylinder, which is valid if there is no slip between the wires. In a helically reinforced cylinder, the CTE is in general anisotropic. At any point on a helical fiber, a local coordinate system $(P; \boldsymbol{\tau}, \mathbf{b}, \mathbf{r})$ is established where $\boldsymbol{\tau}$ is the tangential direction with Cartesian components shown in Eq. (4), and

$$\text{binormal } \mathbf{b} = \cos\beta \sin\phi \mathbf{e}_1 - \cos\beta \cos\phi \mathbf{e}_2 + \sin\beta \mathbf{e}_3 \tag{35}$$

$$\text{radial } \mathbf{r} = \cos\phi \mathbf{e}_1 + \sin\phi \mathbf{e}_2 \tag{36}$$

A temperature increase Θ equivalently causes the following thermal strain:

$$[\boldsymbol{\varepsilon}_{\mathbf{th}}]^{\tau br} = \begin{bmatrix} -\eta_\tau \Theta & 0 & 0 \\ 0 & -\eta_b \Theta & 0 \\ 0 & 0 & -\eta_r \Theta \end{bmatrix} \tag{37}$$

where η_τ, η_b, and η_r are the CTE along the fibers, between fibers within the same layer of helical wires, and between fibers in neighboring layers, respectively. The local thermal strain components are transformed into global components in the Cartesian coordinate system $(O; \mathbf{e}_1, \mathbf{e}_2, \mathbf{e}_3)$ via

$$[\boldsymbol{\varepsilon}_{\mathbf{th}}]^{global} = [Q]^{\mathrm{T}} [\boldsymbol{\varepsilon}_{\mathbf{th}}]^{\tau br} [Q] \tag{38}$$

where $[Q]$ is the transformation matrix. The stress induced by $[\boldsymbol{\varepsilon}_{\mathbf{th}}]^{global}$ can be obtained from Eq. (5), which upon integration following Eq. (8) gives the cross section loads, and thus k_i's:

$$\begin{gathered} k_3 = \pi R^2 k_e \\ k_6 = \pi R^3 k_r \\ k_1 = k_2 = k_4 = k_5 = 0 \end{gathered}$$

where

$$\begin{aligned} k_e = \frac{1}{2}\eta_\tau \big\{ \cos(2\beta)[\alpha_1 + \alpha_2 + 2(\alpha_3 + \mu)] + 3\alpha_1 + \alpha_2 + 2(\alpha_3 + \lambda + \mu) \big\} \\ + \frac{1}{2}\eta_b(\alpha_1 \cos(2\beta) + \alpha_1 - 2\mu\cos(2\beta) + 2\lambda + 2\mu) \\ + \frac{1}{2}\eta_r(\alpha_1 \cos(2\beta) + \alpha_1 + 2\lambda) \end{aligned} \tag{39}$$

and

$$\begin{aligned} k_r = \frac{1}{3}\eta_\tau \sin(2\beta)[\alpha_1 + \alpha_2 + 2(\alpha_3 + \mu)] \\ + \frac{1}{3}\eta_b(\alpha_1 - 2\mu)\sin(2\beta) \\ + \frac{1}{3}\eta_r \alpha_1 \sin(2\beta) \end{aligned} \tag{40}$$

Therefore, the thermal expansion only leads to modifications to the axial force N_3 and moment M_3, while it has no effect on bending and shearing. This is consistent with Eq. (34), but the result here is more general as the anisotropy of CTE is considered. Also different is the fact that in the anisotropic case, one has to use a thermal finite element analysis to estimate the nonzero thermal coefficients, since no simple relation between k_i and C_{ij} is available. Another observation from Eq. (40) is that $k_6 = 0$ when the lay angle $\beta = 0$, and also $k_6 \sim \beta$ when β is small, i.e., k_6 is a result of the presence of helices. In contrast, $k_3 \neq 0$ for zero β. k_e and k_r are coefficients that do not depend on the cross section area of the strand. We further note that when the CTE is not uniform over the cross section, we do not in general have $k_1 = k_2 = k_4 = k_5 = 0$, i.e., there may be coupling between thermal expansion and bending, as is reported in [12]. However, when the variation of CTE is only along the radial direction, we still end up with $k_1 = k_2 = k_4 = k_5 = 0$ following the same derivation as above.

In summary, we have created a generalized Timoshenko model for helical strands with thermal expansion:

$$\begin{Bmatrix} N_1 \\ N_2 \\ N_3 \\ M_1 \\ M_2 \\ M_3 \end{Bmatrix} = \begin{bmatrix} \pi R^2 G_{\mathrm{s}} & 0 & 0 & -\frac{\pi R^3}{2} C_f & 0 & 0 \\ 0 & \pi R^2 G_{\mathrm{s}} & 0 & 0 & -\frac{\pi R^3}{2} C_f & 0 \\ 0 & 0 & \pi R^2 E_{\mathrm{e}} & 0 & 0 & \pi R^3 C_f \\ -\frac{\pi R^3}{2} C_f & 0 & 0 & \frac{\pi R^4}{4} E_{\mathrm{b}} & 0 & 0 \\ 0 & -\frac{\pi R^3}{2} C_f & 0 & 0 & \frac{\pi R^4}{4} E_{\mathrm{b}} & 0 \\ 0 & 0 & \pi R^3 C_f & 0 & 0 & \frac{\pi R^4}{2} G_{\mathrm{r}} \end{bmatrix} \begin{Bmatrix} \gamma_1 \\ \gamma_2 \\ \gamma_3 \\ \kappa_1 \\ \kappa_2 \\ \kappa_3 \end{Bmatrix} - \begin{Bmatrix} 0 \\ 0 \\ \pi R^2 k_e \\ 0 \\ 0 \\ \pi R^3 k_r \end{Bmatrix} \Theta \tag{41}$$

It is governed by five effective elastic moduli G_{s}, E_{e}, E_{b}, G_{r}, and C_f, and two effective thermal coefficients, k_3 and k_6. The values of these constants can be obtained with the procedures mentioned above. Then, the general deformation of the helical strand can be solved with 1D beam equations. We investigate the thermoelastic wave propagation in a helical strand in the following section. It is a modification of our earlier results where the contribution of thermal expansion to the torsional moment was assumed zero.

Thermoelastic wave equations

The Timoshenko rod model can now be employed to study the mechanical wave propagation in a helical strand [22]. The equations of vibration can be separated into two sets uncoupled from each other: one set of two tension–torsion equations and one set of four bending–shearing equations. The eigenvalue problems of the two sets of equations are solved, yielding the dispersion relations and vibration modes. In another article, we studied the thermoelastic waves in a helical strand with the heat transfer following either a parabolic (i.e., Fourier) or a hyperbolic (i.e., Maxwell-Cattaneo) type [21], where the strand was assumed to have tension–torsion coupling, with the thermal expansion only affecting the axial force, not the axial torque. In contradistinction to this, in the thermomechanical constitutive law we derived in the current study (Eq. (41)), one important consequence of the structural chirality is that thermal expansion leads to a change of the axial torque as well. In this study, the thermoelastic wave problem in a helical strand is solved with the rod model proposed above. The heat conduction is assumed to follow Fourier's law, which is sufficient for the majority of engineering applications.

Since the thermal expansion does not affect the bending and shearing loads, and the tension–-torsion problem is also uncoupled from the bending–shearing problem, the bending–shearing equations are excluded in this section, resulting in the following reduced thermomechanical constitutive law

$$N_3 = \pi R^2 E_e u_3' + \pi R^3 C_f \theta_3' - \pi R^2 k_e \Theta \tag{42a}$$

$$M_3 = \pi R^3 C_f u_3' + \frac{1}{2} \pi R^4 G_r \theta_3' - \pi R^3 k_r \Theta \tag{42b}$$

The Fourier heat conduction law states

$$Q = -AK\Theta' \tag{43}$$

where K is the thermal conductivity along the strand's axis, Q is the heat flux in the whole cross section, and A is the area of the cross section. The momentum balance equations are reduced from Eq. (15) to

$$N_3' = \rho A \ddot{u}_3 \tag{44a}$$

$$M_3' = \rho J \ddot{\theta}_3 \tag{44b}$$

where J is the torsional moment of inertia of the cross section. Since we effectively replace a helical strand with a helically reinforced rod with cross section radius R via the constitutive relation Eq. (41), we have

$$A = \pi R^2$$
$$J = \frac{\pi R^4}{2}$$

The equation of entropy rate is

$$T_0 \dot{S} = -Q' \tag{45}$$

where S is the entropy per unit length of the strand and T_0 is a reference temperature such that the instantaneous temperature $T = \Theta + T_0$ [36]. In analogy to the thermoelasticity constitutive theory for linear 3D media [36], the free-energy per unit length of a rod following Eq. (32) can be written as follows:

$$\Psi = \Psi_0 - S_0\Theta + \frac{1}{2}\{\boldsymbol{\gamma}\}^{\mathrm{T}}[\mathbf{C}]\{\boldsymbol{\gamma}\} - \{\boldsymbol{k}\}^{\mathrm{T}}\{\boldsymbol{\gamma}\}\Theta - \frac{\rho c_v A}{2T_0}\Theta^2 \tag{46}$$

Then,

$$S = -\frac{\partial \Psi}{\partial T} = \{\boldsymbol{k}\}^{\mathrm{T}}\{\boldsymbol{\gamma}\} + \frac{\rho c_v A}{T_0}\Theta \tag{47}$$

by properly choosing the reference state entropy value. Substituting Eqs. (43) and (47) into Eq. (45) and assuming $|\Theta| \ll T_0$, we get

$$\frac{T_0}{A}\{\boldsymbol{k}\}^{\mathrm{T}}\{\dot{\boldsymbol{\gamma}}\} + \rho c_v \dot{\Theta} = K\Theta'' \tag{48}$$

which, in view of Eq. (41), is reduced to

$$T_0\left(k_e \dot{u}_3' + k_r R \dot{\theta}_3'\right) + \rho c_v \dot{\Theta} = K\Theta'' \tag{49}$$

Equations (42) and (44) can be combined, which then together with Eq. (49) form the following three coupled equations governing the thermomechanical behavior of the helical strand

$$\rho \ddot{u}_3 = E_e u_3'' + RC_f \theta_3'' - k_e \Theta' \tag{50a}$$

$$\rho \frac{R}{2}\ddot{\theta}_3 = C_f u_3'' + \frac{R}{2} G_r \theta_3'' - k_r \Theta' \tag{50b}$$

$$\rho c_v \dot{\Theta} = K\Theta'' - T_0\left(k_e \dot{u}_3' + k_r R \dot{\theta}_3'\right) \tag{50c}$$

Note that the coupling between torsion and temperature is accounted for here, due to a nonzero k_r, which is neglected in Ref. [21].

Thermoelastic coupling and wave solutions

Assuming the following space-time-harmonic wave form solutions,

$$u_3(x,t) = A^* \exp[ik(x - ct)] \tag{51a}$$

$$\theta_3(x,t) = B^* \exp[ik(x - ct)] \tag{51b}$$

$$\Theta(x,t) = C^* \exp[ik(x - ct)] \tag{51c}$$

we arrive at the dispersion relation

$$\begin{vmatrix} E_e - c^2\rho & C_f R & i\dfrac{k_e}{k} \\ C_f & \dfrac{1}{2}R\left(G_r - c^2\rho\right) & i\dfrac{k_r}{k} \\ \dfrac{ck_eT_0}{\rho c_v} & \dfrac{ck_rRT_0}{\rho c_v} & \dfrac{K}{\rho c_v} - i\dfrac{c}{k} \end{vmatrix} = 0 \tag{52}$$

Note that the matrix is full, due to the thermal coupling with tension and torsion. The solutions of the dispersion relation remain the same if a row or a column is multiplied by a constant. Hence, the following equivalent form is obtained:

$$\begin{vmatrix} 1 - c^2\dfrac{\rho}{E_e} & \sqrt{\epsilon_c} & \sqrt{\epsilon_e} \\ \sqrt{\epsilon_c} & 1 - c^2\dfrac{\rho}{G_r} & \sqrt{\epsilon_r\epsilon_c} \\ \sqrt{\epsilon_e} & \sqrt{\epsilon_r\epsilon_c} & -\left(1 + \dfrac{i\Gamma}{c}\right) \end{vmatrix} = 0 \tag{53}$$

where

$$\eta_e = \frac{k_e}{E_e}, \qquad \eta_r = \frac{k_r}{C_f}, \qquad \Gamma = \frac{kK}{c_v\rho}, \qquad \epsilon_e = \eta_e^2\frac{T_0}{c_v}\frac{E_e}{\rho}, \qquad \epsilon_r = \eta_r^2\frac{T_0}{c_v}\frac{E_e}{\rho}, \qquad \epsilon_c = 2\frac{C_f^2}{E_eG_r}.$$

Note that ϵ_e, ϵ_r and ϵ_c are non-dimensional, while Γ has the unit of celerity. ϵ_c is a measure of chirality ($\epsilon_c = 0$ if the lay angle is 0). ϵ_e and ϵ_r are the thermoelastic coupling factors. For an isotropic straight rod under isothermal condition, the longitudinal wave celerity is $\sqrt{E/\rho}$, and the torsional celerity is $\sqrt{G/\rho}$. If the thermoelastic coupling is considered, then, under an adiabatic condition, the longitudinal celerity is

$$\sqrt{\frac{E}{\rho}(1+\epsilon)}, \quad \text{with } \epsilon = \frac{\eta^2 ET_0}{\rho c_v} \tag{54}$$

while the torsional celerity remains the same [37]. The parameter ϵ represents the thermoelastic coupling. In our case, there is thermal expansion effect in both the longitudinal and the torsional directions due to chirality, quantified by η_e and η_r, respectively. Therefore, we have two thermoelastic coupling factors, ϵ_e and ϵ_r. Γ is the product of the thermal diffusivity $K/c_v\rho$ and the wavenumber k, and thus, a small Γ may correspond to a large wavelength ($k \ll 1$) or low thermal conductivity. As is discussed later, Γ is an important parameter in the transition of the solution from the adiabatic regime to the isothermal regime.

Multiplying Eq. (53) by c we obtain a fifth-order polynomial equation in c with five roots that are in general complex. This polynomial is denoted $\mathcal{F}(c)$ henceforth. The coefficients of the odd-order terms are real and the even-oder terms purely imaginary. For such an equation, if c is a root, then -$\bar{c}$ is a root as well, where $\bar{c}$ is the conjugate of c, i.e., the roots are in pairs $\pm\Re c + \Im c \cdot i$ or a pure imaginary number. It will be seen later that the two pairs of roots $\pm\Re c + \Im c \cdot i$ correspond to the quasi-longitudinal wave and the quasi-torsional wave, whereas the single pure imaginary root corresponds to the thermal field. Here "quasi" means that the longitudinal mode is always coupled with a small torsional motion and vice versa, due to chirality [21,38]. For brevity, we omit "quasi" in the following writing.

According to Eq. (51), $\Re c$ represents the celerity of the wave, and $-k \cdot \Im c$ represents the damping factor. The solutions to $\mathcal{F}(c) = 0$ can be computed numerically in general. However, analytic solutions exist for special cases, which reveal important properties of the waves. We will discuss the analytic solutions below. Before the discussion, it is helpful to rewrite the original

equation $\mathcal{F}(c)$ in the form

$$\mathcal{F}(c) = (c + i\Gamma)\mathcal{Q}(c) - c\ \mathcal{P}(c)$$

where $\mathcal{P}(c)$ and $\mathcal{Q}(c)$ are polynomials in c with real coefficients

$$\begin{aligned} \mathcal{P}(c) &= \left(\frac{E_e}{\rho}\epsilon_e + \frac{G_r}{\rho}\epsilon_c\epsilon_r\right)c^2 - \frac{E_e}{\rho}\frac{G_r}{\rho}\left(\epsilon_e - \epsilon_c\left(2\sqrt{\epsilon_e\epsilon_r} - \epsilon_r\right)\right) \\ \mathcal{Q}(c) &= \left(\frac{E_e}{\rho} - c^2\right)\left(\frac{G_r}{\rho} - c^2\right) - \frac{G_r}{\rho}\frac{E_e}{\rho}\epsilon_c \end{aligned} \tag{55}$$

Case I: No thermal expansion

If there is no thermal expansion, i.e., $\epsilon_e = \epsilon_r = 0$, the mechanical and thermal equations in Eq. (50) are decoupled. We have $\mathcal{F}(c) = (c + i\Gamma)\mathcal{Q}(c)$. The root $-i\Gamma$ is associated with the thermal field. Since the real part is zero ($c_{th}^{(1)} = 0$), this is a purely diffusive solution, with the damping

$$d_{th}^{(1)} = k\Gamma = \frac{K}{c_v\rho}k^2$$

which is proportional to the wavenumber squared and the thermal diffusivity $K/(\rho c_v)$. For mechanical waves the celerities for longitudinal and torsional waves are found as the roots of $\mathcal{Q}(c) = 0$,

$$c_l^{(1)} = \left(\frac{E_e + G_r + \sqrt{(E_e - G_r)^2 + 4E_eG_r\epsilon_c}}{2\rho}\right)^{1/2} \tag{56a}$$

$$c_t^{(1)} = \left(\frac{E_e + G_r - \sqrt{(E_e - G_r)^2 + 4E_eG_r\epsilon_c}}{2\rho}\right)^{1/2} \tag{56b}$$

Because $(E_e - G_r)^2 + 4E_eG_r\epsilon_c > 0$, no damping is present in the elastic waves ($d_l^{(1)} = d_t^{(1)} = 0$). The celerities are consistent with quasi-torsional and quasi-longitudinal wave solutions of a helix obtained in [22,38]. Also note that Γ is not present in the solutions, suggesting the waves are nondispersive and independent of the thermal conductivity.

If the helix has a small lay angle such that $\epsilon_c \ll 1$, a Taylor expansion gives

$$c_l^{(1)} = \sqrt{\frac{E_e}{\rho} + \frac{E_eG_r}{\rho(E_e - G_r)}\epsilon_c} + \mathcal{O}(\epsilon_c^2), \qquad c_t^{(1)} = \sqrt{\frac{G_r}{\rho} - \frac{E_eG_r}{\rho(E_e - G_r)}\epsilon_c} + \mathcal{O}(\epsilon_c^2) \tag{57}$$

Case II: Asymptotics using small thermoelastic coupling condition

When $\epsilon_r \neq 0, \epsilon_e \neq 0$, but $\epsilon_e \ll 1$ and $\epsilon_r \ll 1$, there is a weak thermoelastic coupling. This is in particular true for a small coefficient of thermal expansion, which is the case for many engineering materials. The effect of the thermoelastic coupling on the wave solutions can then be introduced as a perturbation term.

Perturbation method

Consider a solution $c^{(1)}$ for the problem with $\epsilon_e = \epsilon_r = 0$. The new solution can be written as $c = c^{(1)} + \delta c + \mathcal{O}(\epsilon_{e,r}^2)$. Here, $\mathcal{O}(\epsilon_{e,r}^2)$ means that δc is of the same order of magnitude as ϵ_e, ϵ_r or $\sqrt{\epsilon_e\epsilon_r}$, with δc to be solved. A Taylor series expansion of $\mathcal{F}$ up to the first order in the neighborhood of $c^{(1)}$ gives

$$\mathcal{F}\left(c^{(1)}+\delta c\right) \approx \mathcal{F}\left(c^{(1)}\right)+\delta c \left.\frac{\partial \mathcal{F}}{\partial c}\right|_{c=c^{(1)}} \tag{58}$$

$$=\left(c^{(1)}+i\Gamma\right)\mathcal{Q}\left(c^{(1)}\right)-c^{(1)}\mathcal{P}\left(c^{(1)}\right)+\delta c \left.\frac{\partial \mathcal{F}}{\partial c}\right|_{c=c^{(1)}} \tag{59}$$

$$=-c^{(1)}\mathcal{P}\left(c^{(1)}\right)+\delta c \left.\frac{\partial \mathcal{F}}{\partial c}\right|_{c=c^{(1)}} \tag{60}$$

where the last equality is from the definition of $c^{(1)}$. The quantities $-c^{(1)}\mathcal{P}(c^{(1)})$ and $\partial\mathcal{F}/\partial c|_{c=c^{(1)}}$ are functions of ϵ_e and ϵ_r. As $\epsilon_e \ll 1$ and $\epsilon_r \ll 1$, it is sufficient to solve Eq. (58) to the first order in ϵ_e and ϵ_r, giving a linear relation in terms of δc that can be solved analytically:

$$\delta c \left.\frac{\partial (c+i\Gamma)\mathcal{Q}(c)}{\partial c}\right|_{c=c^{(1)}} = c^{(1)}\mathcal{P}\left(c^{(1)}\right) \tag{61}$$

This procedure is conducted with respect to each root for the case of zero thermal expansion, $c_l^{(1)}, c_t^{(1)}$, and $-i\Gamma$.

Elastic field

With Eqs. (61) and (55), the perturbations for the longitudinal and torsional wave solutions are

$$\delta c = c\frac{\mathcal{P}(c)}{(c+i\Gamma)\frac{\partial \mathcal{Q}}{\partial c}} = \frac{\left(\frac{E_e}{\rho}\epsilon_e+\frac{G_r}{\rho}\epsilon_c\epsilon_r\right)c^2-\frac{E_e}{\rho}\frac{G_r}{\rho}\left(\epsilon_e-\epsilon_c\left(2\sqrt{\epsilon_e\epsilon_r}-\epsilon_r\right)\right)}{4(c+i\Gamma)\left(c^2-\frac{E_e+G_r}{2\rho}\right)} \tag{62}$$

with $c=c_l^{(1)}$ or $c_t^{(1)}$, respectively. This solution contains an imaginary coefficient through $(c+i\Gamma)^{-1}$, hence there is damping in the elastic waves. Since all other variables are real, the amount of damping is controlled by Γ. In particular, two situations are considered, $\Gamma \ll c$ (where $c=c_l^{(1)}$, or $c_t^{(1)}$), and $\Gamma \gg c$. The physical meanings of these two conditions can be elucidated with the Fourier number. The Fourier number is defined as $\mathrm{Fo}=DT_c/L_c^2$ where $D=K/c_v\rho$ is the thermal diffusivity, T_c is the characteristic time scale, and L_c the characteristic length scale. For the wave-form solution Eq. (51), the time scale is $T_c=2\pi/\omega=2\pi/ck$ and the length scale is the wavelength $L_c=2\pi/k$, so

$$\mathrm{Fo}=\frac{1}{2\pi}\frac{Kk}{c_v\rho c}=\frac{1}{2\pi}\frac{\Gamma}{c} \tag{63}$$

Therefore, the condition $\Gamma \ll c$ is equivalent to $\mathrm{Fo} \ll 1$. It corresponds to the case where elastic wave propagation dominates the thermal diffusion, i.e., it is an adiabatic process. On the other hand, $\Gamma \gg c$ is equivalent to $\mathrm{Fo} \gg 1$, representing the case where thermal diffusion dominates the elastic wave propagation, i.e., it is an isothermal process. We define the wavenumber such that $\Gamma = c$ as the critical wavenumber,

$$k_{cr}=\frac{\rho c_v c}{K} \tag{64}$$

which can used to estimate where the adiabatic-isothermal transition occurs as the wavenumber varies. Similarly, we have the critical frequency

$$\omega_{cr}=k_{cr}c=\frac{\rho c_v c^2}{K} \tag{65}$$

In practice, c in Eqs. (63)–(65) is a characteristic celerity, and one can also use $\sqrt{E_e/\rho}$ (for longitudinal waves) and $\sqrt{G_r/\rho}$ (for torsional waves), instead of Eq. (56), as they are typically of the same order of magnitude.

1. **Adiabatic regime:** If $\Gamma \ll c$, then in Eq. (61) the following Taylor series expansion is used $(c+i\Gamma)^{-1} = \frac{1}{c}(1-i\frac{\Gamma}{c}) + \mathcal{O}((\frac{\Gamma}{c})^2)$. The wave celerity and damping become

$$\begin{aligned} c_{l,t}^{(2)} &= c + \frac{\left(\frac{E_e}{\rho}\epsilon_e + \frac{G_r}{\rho}\epsilon_c\epsilon_r\right)c^2 - \frac{E_e}{\rho}\frac{G_r}{\rho}\left(\epsilon_e - \epsilon_c\left(2\sqrt{\epsilon_e\epsilon_r} - \epsilon_r\right)\right)}{4c\left(c^2 - \frac{E_e+G_r}{2\rho}\right)} \\ d_{l,t}^{(2)} &= \frac{k\Gamma}{c^2}\frac{\left(\frac{E_e}{\rho}\epsilon_e + \frac{G_r}{\rho}\epsilon_c\epsilon_r\right)c^2 - \frac{E_e}{\rho}\frac{G_r}{\rho}\left(\epsilon_e - \epsilon_c\left(2\sqrt{\epsilon_e\epsilon_r} - \epsilon_r\right)\right)}{4\left(c^2 - \frac{E_e+G_r}{2\rho}\right)} \end{aligned} \tag{66}$$

where, on the right-hand side, $c = c_l^{(1)}$ or $c_t^{(1)}$ for the longitudinal and torsional waves respectively. As ϵ_e and ϵ_r are both proportional to T_0, the celerity is linearly dependent on the temperature and the damping is proportional to the temperature. The celerity is independent of Γ, hence the waves are nondispersive. However, the damping of the elastic waves is proportional to K and k^2. For isotropic thermal expansion, $\epsilon_r = \epsilon_e$, the elastic damping and celerity are simplified to

$$\begin{aligned} c_{l,t}^{(2)} &= c + \epsilon_e\frac{\left(\frac{E_e}{\rho} + \frac{G_r}{\rho}\epsilon_c\right)c^2 - \frac{E_e}{\rho}\frac{G_r}{\rho}(1-\epsilon_c)}{4c\left(c^2 - \frac{E_e+G_r}{2\rho}\right)} \\ d_{l,t}^{(2)} &= \frac{k\Gamma}{c^2}\epsilon_e\frac{\left(\frac{E_e}{\rho} + \frac{G_r}{\rho}\epsilon_c\right)c^2 - \frac{E_e}{\rho}\frac{G_r}{\rho}(1-\epsilon_c)}{4\left(c^2 - \frac{E_e+G_r}{2\rho}\right)} \end{aligned}$$

To demonstrate the effect of the lay angle, we take a first-order expansion of Eq. (66) in the limit of $\epsilon_c \ll 1$, to get

$$c_l^{(2)} \approx \sqrt{\frac{E_e}{\rho}}\left(1 + \frac{\epsilon_e}{2} + \frac{\epsilon_c}{2}\frac{G_r}{E_e - G_r}\left(1 - \frac{\epsilon_e}{2}\frac{3E_e - G_r}{E_e - G_r} + 2\sqrt{\epsilon_e\epsilon_r}\right)\right) \tag{67a}$$

$$c_t^{(2)} \approx \sqrt{\frac{G_r}{\rho}}\left(1 + \frac{\epsilon_c\epsilon_r}{2} + \frac{E_e}{(E_e - G_r)^2}\frac{\epsilon_c}{2}\left(G_r\left(1 + 2\sqrt{\epsilon_e\epsilon_r}\right) - E_e\left(1 - \epsilon_e + 2\sqrt{\epsilon_r\epsilon_e}\right)\right)\right) \tag{67b}$$

$$d_l^{(2)} \approx \frac{1}{2}k\Gamma\left(\epsilon_e + \epsilon_c\sqrt{\epsilon_e}\frac{G_r}{(E_e - G_r)^2}\left(2\sqrt{\epsilon_r}(E_e - G_r) + \sqrt{\epsilon_e}(G_r - 2E_e)\right)\right) \tag{67c}$$

$$d_t^{(2)} \approx \frac{1}{2}k\Gamma\epsilon_c\left(\sqrt{\epsilon_r} - \frac{E_e}{E_e - G_r}\sqrt{\epsilon_e}\right)^2 \tag{67d}$$

If we neglect the quadratic terms $\mathcal{O}(\epsilon_c\epsilon_e)$ and $\mathcal{O}(\epsilon_c\epsilon_r)$, Eq. (67) can be written as

$$c_l^{(2)} \approx c_l^{(1)} + \sqrt{\frac{E_e}{\rho}}\frac{\epsilon_e}{2}, \quad d_l^{(2)} \approx \frac{1}{2}k\Gamma\epsilon_e \tag{68a}$$

$$c_t^{(2)} \approx c_t^{(1)}, \quad d_t^{(2)} \approx 0 \tag{68b}$$

In other words, in the case of weak chirality and thermoelastic coupling, the longitudinal thermoelastic coupling has a more significant effect on the longitudinal waves than on the torsional waves, and the effect of torsional thermoelastic coupling is negligible on both waves. For isotropic thermal expansion, the dampings for the longitudinal and torsional waves in Eq. (67) are further simplified to

$$d_l^{(2)} = \frac{1}{2}k\Gamma\epsilon_e\left(1-\epsilon_c\left(\frac{G_r}{E_e-G_r}\right)^2\right), \qquad d_t^{(2)} = \frac{1}{2}k\Gamma\epsilon_e\epsilon_c\left(\frac{G_r}{E_e-G_r}\right)^2 \tag{69}$$

Since ϵ_c is always positive, it is observed from Eq. (69) that the chirality reduces the damping of the longitudinal wave and increases the damping of the torsional wave by the same amount. If we use the first-order approximation $k \approx \omega/c_l^{(1)}$ for longitudinal waves and $k \approx \omega/c_t^{(1)}$ for torsional waves in Eq. (69), then we also have the dampings in terms of the frequency ω

$$d_l^{(2)} = \omega^2\frac{KT_0\eta_e^2}{\rho c_v^2}\frac{1}{2}\left(1-2\left(\frac{C_f}{E_e-G_r}\right)^2\right)$$
$$d_t^{(2)} = \omega^2\frac{KT_0\eta_e^2}{\rho c_v^2}\left(\frac{C_f}{E_e-G_r}\right)^2$$

2. **Isothermal regime:** If $\Gamma \gg c$, then in Eq. (61) the Taylor series expansion $(c+i\Gamma)^{-1} = -\frac{i}{\Gamma}-\frac{c}{\Gamma^2}+\mathcal{O}((\frac{c}{\Gamma})^2)$ is used. If we neglect terms of quadratic or higher orders in c/Γ, then we see the wave celerities are the same as those found in the case of no thermal expansion (Eq. (56)), i.e.,

$$c_l^{(3)} \approx c_l^{(1)}, \qquad c_t^{(3)} \approx c_t^{(1)}. \tag{70}$$

However, there is nonzero damping here,

$$d_{l,t}^{(3)} = \frac{k}{\Gamma}\frac{\left(\frac{E_e}{\rho}\epsilon_e+\frac{G_r}{\rho}\epsilon_c\epsilon_r\right)c^2-\frac{E_e}{\rho}\frac{G_r}{\rho}\left(\epsilon_e-\epsilon_c\left(2\sqrt{\epsilon_e\epsilon_r}-\epsilon_r\right)\right)}{4\left(c^2-\frac{E_e+G_r}{2\rho}\right)} \tag{71}$$

where $c = c_l^{(1)}$, or $c_t^{(1)}$, depending on whether the wave is longitudinal or torsional. Because $k/\Gamma = c_v\rho/K$, the damping is independent of the wavenumber. Same as for the adiabatic regime, the damping is proportional to the temperature T_0. It is noticed that Eq. (71) is essentially the same as its adiabatic counterpart in Eq. (66) if the coefficient k/Γ is replaced with $k\Gamma/c^2$. For isotropic thermal expansion, the elastic damping is

$$d_{l,t}^{(3)} = \frac{k}{\Gamma}\epsilon_e\frac{\left(\frac{E_e}{\rho}+\frac{G_r}{\rho}\epsilon_c\right)c^2-\frac{E_e}{\rho}\frac{G_r}{\rho}(1-\epsilon_c)}{4\left(c^2-\frac{E_e+G_r}{2\rho}\right)}$$

which in the case of weak chirality, is further simplified to:

$$d_l^{(3)} = \frac{1}{2}\frac{E_e}{\rho}\frac{k}{\Gamma}\epsilon_e = \frac{1}{2}E_e^2\ \eta_e^2\frac{T_0}{K\rho}$$
$$d_t^{(3)} = \frac{1}{2}\frac{G_r^3}{\rho(E_e-G_r)^2}\frac{k}{\Gamma}\epsilon_c\epsilon_e = \left(\frac{C_fG_r}{E_e-G_r}\right)^2\ \eta_e^2\frac{T_0}{K\rho}$$

It is observed that c_v does not affect damping in the isothermal regime.

Table 5. Asymptotic behavior of the solutions.

	Adiabatic	Isothermal
Condition	$\omega \ll \frac{c_v\rho}{K}c^2, k \ll \frac{c_v\rho}{K}c, Fo \ll 1$	$\omega \gg \frac{c_v\rho}{K}c^2, k \gg \frac{c_v\rho}{K}c, Fo \gg 1$
Celerity ($\epsilon_e, \epsilon_r \ll 1$)	$c_l^{(2)}$ and $c_t^{(2)}$ (Eq. 66)	$c_l^{(1)}$ and $c_t^{(1)}$ (Eq. 56)
	Independent of k, non-dispersive	Independent of k, non-dispersive
	Linear in T_0	Independent of T_0
Celerity (ϵ_e, ϵ_r finite)	$c_l^{(4)}$ and $c_t^{(4)}$ (Eq. 76)	$c_l^{(1)}$ and $c_t^{(1)}$ (Eq. 56)
	Independent of k, non-dispersive	Independent of k, non-dispersive
	Dependent on T_0	Independent of T_0
Damping ($\epsilon_e, \epsilon_r \ll 1$)	$d_l^{(2)}$ and $d_t^{(2)}$ (Eq. 66)	$d_l^{(3)}$ and $d_t^{(3)}$ (Eq. 71)
	Proportional to k^2	Independent of k
	Proportional to T_0	Proportional to T_0
Damping (ϵ_e, ϵ_r finite)	$d_l^{(4)}$ and $d_t^{(4)}$ (Eq. 76)	$d_l^{(5)}$ and $d_t^{(5)}$ (Eq. 78)
	Proportional to k^2	Independent of k
	Dependent on T_0	Proportional to T_0

Thermal field

For the thermal field, the perturbation to $c^{(1)} = -i\Gamma$ is

$$\delta c = -i\Gamma \frac{\mathcal{P}(-i\Gamma)}{\mathcal{Q}(-i\Gamma)} = i\Gamma \frac{\left(\frac{E_e}{\rho}\epsilon_e + \frac{G_r}{\rho}\epsilon_c\epsilon_r\right)\Gamma^2 + \frac{E_e}{\rho}\frac{G_r}{\rho}\left(\epsilon_e - \epsilon_c\left(2\sqrt{\epsilon_e\epsilon_r} - \epsilon_r\right)\right)}{\left(\frac{E_e}{\rho} + \Gamma^2\right)\left(\frac{G_r}{\rho} + \Gamma^2\right) - \frac{G_r}{\rho}\frac{E_e}{\rho}\epsilon_c}$$

It is purely imaginary, suggesting there is no propagation of the thermal field. The thermal damping is

$$d_{th}^{(2)} = k\Gamma\left(1 - \frac{\left(\frac{E_e}{\rho}\epsilon_e + \frac{G_r}{\rho}\epsilon_c\epsilon_r\right)\Gamma^2 + \frac{E_e}{\rho}\frac{G_r}{\rho}\left(\epsilon_e - \epsilon_c\left(2\sqrt{\epsilon_e\epsilon_r} - \epsilon_r\right)\right)}{\left(\frac{E_e}{\rho} + \Gamma^2\right)\left(\frac{G_r}{\rho} + \Gamma^2\right) - \frac{G_r}{\rho}\frac{E_e}{\rho}\epsilon_c}\right) \tag{72}$$

which is proportional to k^2. If the thermal expansion is isotropic, i.e., $\epsilon_r = \epsilon_e$, the damping is simplified to

$$d_{th}^{(2)} = k\Gamma\left(1 - \epsilon_e\frac{\left(\frac{E_e}{\rho} + \frac{G_r}{\rho}\epsilon_c\right)\Gamma^2 + \frac{E_e}{\rho}\frac{G_r}{\rho}(1 - \epsilon_c)}{\left(\frac{E_e}{\rho} + \Gamma^2\right)\left(\frac{G_r}{\rho} + \Gamma^2\right) - \frac{G_r}{\rho}\frac{E_e}{\rho}\epsilon_c}\right)$$

In the adiabatic regime, $\Gamma \ll \sqrt{\frac{E_e}{\rho}}$ and $\Gamma \ll \sqrt{\frac{G_r}{\rho}}$. The thermal damping Eq. (72) can be represented in the first-order approximation as follows:

$$d_{th}^{(2)} \approx k\Gamma \quad 1 - \frac{\epsilon_e - \epsilon_c\left(2\sqrt{\epsilon_e\epsilon_r} - \epsilon_r\right)}{1 - \epsilon_c}\Bigg)$$

and for isotropic thermal expansion,

$$d_{th}^{(2)} \approx k\Gamma(1 - \epsilon_e) \tag{73}$$

In the isothermal regime, $d_{th}^{(2)} \approx k\Gamma$ in the first-order approximation for both anisotropic and isotropic thermal expansions.

Case III: Asymptotics without using small thermoelastic coupling condition

When ϵ_e and ϵ_r are not small, the solutions cannot be obtained with the perturbation method. However, we can still consider the solutions in the adiabatic or the isothermal regimes. We notice that the dispersion relation Eq. (53) can be further nondimensionalized by introducing,

Table 6. Values of additional properties of the steel strand to be used for celerity calculation.

Property	Actual	Equation	Effective
Density	7.8×10^3 kg/m^3	$\rho = \rho_{\text{actual}} \frac{\pi r_0^2 + 6\pi r_1^2}{\pi R^2}$	5.94×10^3 kg/m^3
Thermal conductivity	50 W/(mK)	$K = K_{\text{actual}} \frac{\pi r_0^2 + 6\pi r_1^2}{\pi R^2}$	38 W/(mK)
Specific heat	500 J/(kgK)	$c_v = c_{v,\text{actual}}$	500 J/(kgK)

$$\text{Fo} = \frac{1}{2\pi} \frac{\Gamma}{\sqrt{E_e/\rho}}, \quad c^* = \frac{c}{\sqrt{E_e/\rho}}. \tag{74}$$

According to the discussions above, the wave propagation is an adiabatic process when $\text{Fo} \ll 1$. In that case, the solution c^* can be written as an asymptotic expansion with respect to Fo:

$$c^* = c_0^* + c_1^* \text{Fo} + \mathcal{O}(\text{Fo}^2) \tag{75}$$

Substituting Eq. (75) into the dispersion relation, and setting the leading two terms to zero, we can get explicit solutions for c_0^* and c_1^*. It is found that c_0^* is real and c_1^* is purely imaginary. Therefore, the leading term for celerity is $c_0^* \sqrt{E_e/\rho}$, and the leading term for damping is $-2\pi k \cdot \text{Fo} \cdot \Im(c_1^*) \cdot \sqrt{E_e/\rho}$. Thus, we get the following celerity and damping:

$$c_l^{(4)} = \left\{ \frac{1}{2\rho} \left(E_e(1+\epsilon_e) + G_r(1+\epsilon_c\epsilon_r) + \Big[E_e^2(1+\epsilon_e)^2 + G_r^2(1+\epsilon_c\epsilon_r)^2 \right. \right.$$
$$\left. \left. -2E_eG_r\big(1+\epsilon_e-2\epsilon_c-4\sqrt{\epsilon_e\epsilon_r}\epsilon_c+\epsilon_c\epsilon_r-\epsilon_c\epsilon_e\epsilon_r\big) \Big]^{1/2} \right) \right\}^{1/2} \tag{76a}$$

$$c_t^{(4)} = \left\{ \frac{1}{2\rho} \left(E_e(1+\epsilon_e) + G_r(1+\epsilon_c\epsilon_r) - \Big[E_e^2(1+\epsilon_e)^2 + G_r^2(1+\epsilon_c\epsilon_r)^2 \right. \right.$$
$$\left. \left. -2E_eG_r\big(1+\epsilon_e-2\epsilon_c-4\sqrt{\epsilon_e\epsilon_r}\epsilon_c+\epsilon_c\epsilon_r-\epsilon_c\epsilon_e\epsilon_r\big) \Big]^{1/2} \right) \right\}^{1/2} \tag{76b}$$

$$d_{l,t}^{(4)} = \frac{k\Gamma}{2} \cdot \frac{E_e + G_r - \frac{E_eG_r(1-\epsilon_c)}{c^2\rho} - c^2\rho}{E_e(1+\epsilon_e) + G_r(1+\epsilon_c\epsilon_r) - 2c^2\rho}, \quad \text{with } c = c_l^{(4)} \text{ or } c_t^{(4)} \tag{76c}$$

Upon taking the limit of $\epsilon_e, \epsilon_r \ll 1$, Eq. (76) reduces to Eq. (66). Same as for weak thermoelastic coupling, the celerities are also independent of the wavenumber, and the dampings are proportional to k^2. However, it is no longer the case that the celerities are linear in T_0 and the dampings are proportional to T_0. It was the case for adiabatic waves with weak thermoelastic coupling simply because we assumed $\epsilon_e, \epsilon_r \ll 1$.

On the other hand, the waves are isothermal when $\text{Fo} \gg 1$. An asymptotic expansion of the solution with respect to $1/\text{Fo}$ is pursued:

$$c^* = c_0^* + \frac{c_1^*}{\text{Fo}} + \mathcal{O}\left(\frac{1}{\text{Fo}^2}\right) \tag{77}$$

Following the same procedure as above, we again find c_0^* real and c_1^* purely imaginary. The leading term for celerity is $c_0^* \sqrt{E_e/\rho}$, and the leading term for damping is $-k\Im(c_1^*) \cdot \sqrt{E_e/\rho}/(2\pi \cdot \text{Fo})$. The final solutions are

$$c_l^{(5)} = c_l^{(1)}, \quad c_t^{(5)} = c_t^{(1)} \tag{78a}$$

$$d_l^{(5)} = \frac{k}{4\Gamma\rho\sqrt{4E_eG_r\epsilon_c + (E_e - G_r)^2}} \cdot \left\{ \epsilon_e \left(E_e^2 + E_e\sqrt{4E_eG_r\epsilon_c + (E_e - G_r)^2} - E_eG_r \right) \right.$$

Table 7. The mechanical celerities in different special cases.

Case	Longitudinal		Torsional	
	Equation	Celerity (m/s)	Equation	Celerity (m/s)
No helix, no thermal expansion	$\sqrt{E_e/\rho}$	4553.49	$\sqrt{G_r/\rho}$	1646.81
No expansion, or isothermal	Eq. (56a)	4679.52	Eq. (56b)	1244.30
Adiabatic	Eq. (66)	4683.60 at 293 K	Eq. (66)	1244.31 at 293 K
		4686.10 at 473 K		1244.31 at 473 K

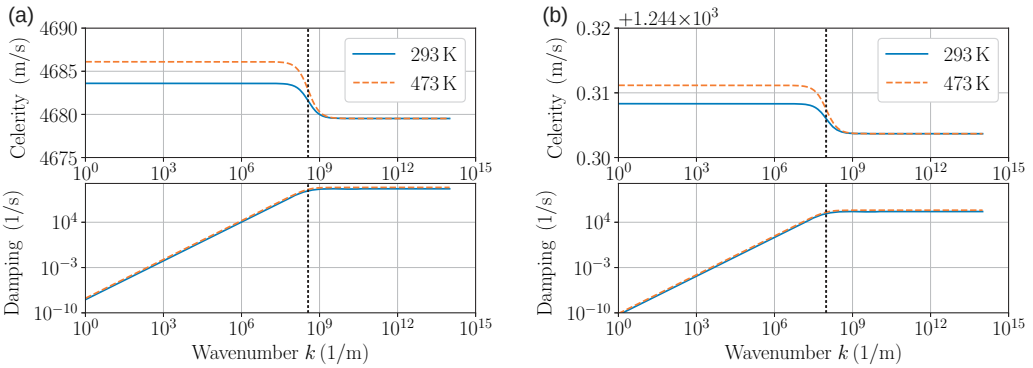

Figure 3. Numerical solutions for (a) longitudinal waves and (b) torsional waves at different temperatures. The critical wavenumbers for adiabatic-isothermal transition computed with Eq. (64) are indicated by the vertical dotted lines. Note the transitions for the longitudinal and the torsional waves do not occur at the same wavenumber.

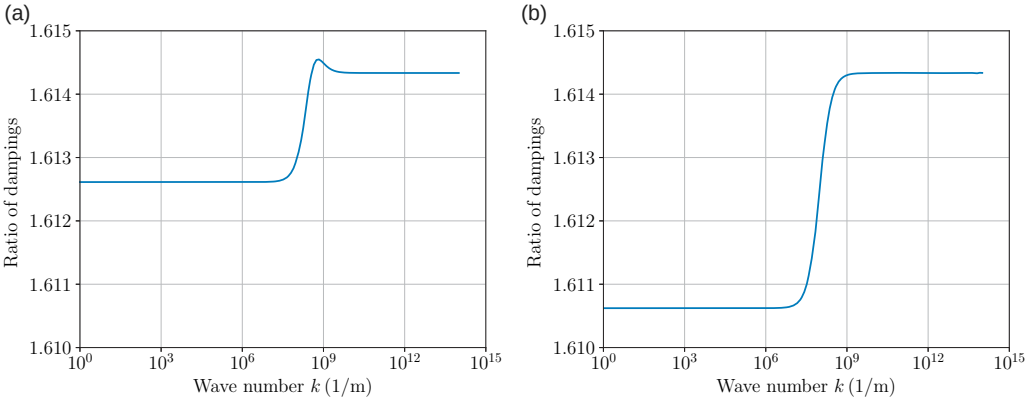

Figure 4. The ratio between the dampings at $T_0 = 473$ K and at $T_0 = 293$ K: (a) longitudinal waves and (b) torsional waves.

$$+\epsilon_r\left(-E_eG_r\epsilon_c + G_r\epsilon_c\sqrt{4E_eG_r\epsilon_c + (E_e-G_r)^2} + G_r^2\epsilon_c\right) + 4E_eG_r\epsilon_c\sqrt{\epsilon_e\epsilon_r}\Bigg\} \tag{78b}$$

$$d_t^{(5)} = \frac{k}{4\Gamma\rho\sqrt{4E_eG_r\epsilon_c + (E_e-G_r)^2}} \cdot \Bigg\{\epsilon_e\left(-E_e^2 + E_e\sqrt{4E_eG_r\epsilon_c + (E_e-G_r)^2} + E_eG_r\right)$$
$$+\epsilon_r\left(E_eG_r\epsilon_c + G_r\epsilon_c\sqrt{4E_eG_r\epsilon_c + (E_e-G_r)^2} - G_r^2\epsilon_c\right) - 4E_eG_r\epsilon_c\sqrt{\epsilon_e\epsilon_r}\Bigg\} \tag{78c}$$

With the definition $\Gamma = kK/(\rho c_v)$, the dampings are independent of k. The dampings are also proportional to T_0 in view of the definitions of ϵ_e and ϵ_r.

The asymptotic behaviors of the solutions in the adiabatic and the isothermal regimes are summarized in Table 5. Note that while the waves in either the adiabatic or the isothermal regimes are nondispersive, the waves between these two limits are in general dispersive.

Numerical example

As a numerical example, we take the values of the moduli E_e, G_r, C_f, k_e, and k_r of the $\beta = 17^\circ$ steel strand from the finite element analysis above. The effective density, thermal conductivity and specific heat are listed in Table 6.

According to these values we have $\epsilon_e = \epsilon_r = 1.75 \times 10^{-3}$ at $T_0 = 293$ K, $\epsilon_e = \epsilon_r = 2.83 \times 10^{-3}$ at $T_0 = 473$ K, and $\epsilon_c = 0.397$. Therefore, we can use the condition of weak thermoelastic coupling $\epsilon_e \ll 1$, but not weak chirality $\epsilon_c \ll 1$. The critical wavenumber for the adiabatic-isothermal transition k_{cr} is estimated as 3.5×10^8 m^{-1} using $c = \sqrt{E_e/\rho}$. It is well beyond the range of wavenumbers for practical purposes. In fact, it corresponds to a wavelength $2\pi/k = 1.7 \times 10^{-8}$ m, which is too low for the rod model to be valid (since the radius $R = 5.7$ mm is much larger than the wavelength). In terms of frequency, the transition occurs around $f = k_{cr}c/2\pi \approx 250$ GHz, which is much higher than frequencies in practical applications. Therefore, the thermoelastic waves in the steel strand are essentially adiabatic. However, it is possible to reach the isothermal regime with a helical strand of a different material or structure. In particular, the isothermal regime is more likely to be achieved for a material with low elastic moduli, low density and high thermal conductivity, and a strand with a large lay angle, or a submicron cross section. The numerical results of the celerities under different special cases for the steel strand are shown in Table 7. It is observed that the torsional celerity is almost unchanged with the isothermal-adiabatic transition, which is consistent with Eq. (68) though ϵ_c is not so small in this case. The longitudinal celerity increases by $\sim$4m/s with the transition at 293 K, which is small, but experimentally measurable. The amount of increase is also comparable with the celerity difference estimated from Eq. (68): 3.98m/s.

To obtain solutions in general cases (away from the adiabatic, or isothermal limits), numerical methods are needed to solve Eq. (53). The numerical solutions of celerities and dampings are shown as functions of the wavenumber in Figure 3. As the asymptotic analysis has shown, the celerities approach the adiabatic solutions for small wavenumbers, and approach the isothermal solutions for large wavenumbers. This is because thermal equilibrium can be established quickly for short waves but slowly for long waves [13,39]. It is also seen from the figure that the damping scales as k^2, for small k's, and plateaus for large k's, consistent with the result of the asymptotic analysis. The dampings are extremely small (as low as $10^{-11} \sim 10^{-8}$ s^{-1}) for this range of wavenumbers. Therefore, the thermoelastic damping is negligible and mechanical damping is more important.

Next, the temperature effects on the thermoelastic waves are investigated. The main consideration is that, with novel designs of overhead power transmission lines, operating temperatures can reach 200$-$250 $^\circ$C [40]. The dampings in both the longitudinal waves and the torsional waves increase by a factor of about 1.6 with the temperature increasing from 293 K to 473 K for our steel strand (Figure 4). But such an increase does not bring a fundamental difference in the damping behavior, as the absolute values of the dampings remain negligible, as shown in Figure 3. Overall, the numerical results show that for the steel strand, the errors of neglecting the thermodynamics and the thermal expansion are very small when compared with the alterations of the celerity brought about by pure tension–torsion coupling. Thermoelastic damping is essentially almost absent for practical applications, and mechanical damping is the dominant source of damping. These results are expected, as they support the use of pure mechanical equations for wave propagations in helical strands for most engineering applications. However, the

thermomechanical coupling effect can be large for high temperature applications, or materials with a high coefficient of thermal expansion, as either case leads to large thermoelastic coupling constants.

It is worth comparing the results we obtained above for a helical strand with the solutions for thermoelastic waves in an isotropic elastic medium [41]. Both solutions approach the adiabatic limit for long waves and the isothermal limit for short waves. In both cases, the longitudinal waves are dispersive and damped. However, there are fundamental differences in our solutions due to the helical structure. In an isotropic medium, the transverse waves do not interact with the temperature field, and only the longitudinal waves are coupled with thermodynamics. As a result, the transverse waves are nondispersive and undamped. In contrast, in the helical medium, the torsional waves (which are a 1 D form of transverse waves) are also coupled with the temperature field, and thus are also dispersive and damped.

Conclusion

In this study, a helical strand without internal slip is modeled as a generalized Timoshenko rod. In a most general Timoshenko rod model, the cross section force and moment components are related to the local deformation by a full 6×6 stiffness matrix. For the helical strand, we identify the zero entries in the stiffness matrix, following a similar procedure to the one we used for [22], which is based on the assumption that the helical strand has the same structural symmetry as a helically reinforced continuum. The model is then extended by introducing thermal expansion terms into the constitutive relation. In the end, we arrive at a thermomechanical constitutive relation with five effective moduli, E_{e} (extension), E_{b} (bending), C_f (coupling), G_{s} (shearing) and G_r (torsion) and two thermal coefficients, k_3 (extensional-thermal coupling) and k_6 (torsional-thermal coupling). In the stiffness matrix, bending–shearing is uncoupled from tension–torsion. The bending–shearing coupling and tension–torsion coupling are both characterized by the coupling moduli C_f. Thermal expansion only affects the axial force and the torsional moment, but not the bending moments and transverse shear forces. In particular, the effect of thermal expansion on the torsional moment is rooted in the presence of helices, and it vanishes when the lay angle reaches zero. For a specific helical strand structure, the values of the effective moduli can be obtained with finite element analysis, or partially, from analytic solutions.

The non-classical bending behavior of helical strands in which an out-of-plane bending moment or transverse force is required to maintain a planar deflection, is predicted by the Timoshenko model and also verified by finite element analysis on a $1+6$ strand structure. The nonclassical bending response is due to the bending–shearing coupling in helical strands, which is considered in the constitutive relation of the Timoshenko rod model. As a comparison, the Euler–Bernoulli model wrongly predicts those out-of-plane load components to be zero as the bending–shearing coupling is neglected.

Other than the bending–shearing coupling, the chirality in helical strands causes a coupling between the torsional deformation and the temperature field, which is also explicitly included in the constitutive relation of the Timoshenko rod model. The harmonic thermoelastic waves in helical strands are solved with this model. The dispersion relation is governed by four nondimensional parameters: two thermoelastic coupling constants, ϵ_e and ϵ_r, one chirality parameter ϵ_c, and the Fourier number Fo. Both the quasi-longitudinal and quasi-torsional waves are dispersive and damped. The dampings originate from the extensional-thermal and torsional-thermal couplings. The celerities of short waves approach the isothermal limit, and long waves the adiabatic limit. More generally, the adiabatic-isothermal transition is controlled by the Fourier number: the solutions are in the adiabatic regime for $\mathrm{Fo} \ll 1$, and in the isothermal regime for $\mathrm{Fo} \gg 1$. The dampings of the waves increase with the wavenumber and eventually plateau as the wavenumber grows to infinity.

Funding

This material is based upon work partially supported by the NSF under grant IIP-1362146 (I/UCRC on Novel High Voltage/Temperature Materials and Structures).

References

[1] T. C. Gasser, R. W. Ogden, and G. A. Holzapfel, "Hyperelastic modelling of arterial layers with distributed collagen fibre orientations," *J. Roy. Soc. Interface*, vol. 3, no. 6, pp. 15–35, 2006.

[2] C. Jolicoeur, "Comparative study of two semicontinuous models for wire strand analysis," *J. Eng. Mech.*, vol. 123, no. 8, pp. 792–799, 1997.

[3] A. Cardou, and C. Jolicoeur, "Mechanical models of helical strands," *Appl. Mech. Rev.*, vol. 50, no. 1, pp. 1–14, 1997.

[4] K. Spak, G. Agnes, and D. Inman, "Cable modeling and internal damping developments," *Appl. Mech. Rev.*, vol. 65, no. 1, pp. 010801, 2013.

[5] J. Lanteigne, "Theoretical estimation of the response of helically armored cables to tension, torsion, and bending," *J. Appl. Mech.*, vol. 52, no. 2, pp. 423–432, 1985.

[6] C. Jolicoeur, and A. Cardou, "Analytical solution for bending of coaxial orthotropic cylinders," *J. Eng. Mech.*, vol. 120, no. 12, pp. 2556–2574, 1994.

[7] J. A. Crossley, A. H. England, and A. J. M. Spencer, "Bending and flexure of cylindrically monoclinic elastic cylinders," *Int. J. Solids Struct.*, vol. 40, no. 25, pp. 6999–7013, 2003.

[8] J. A. Crossley, A. J. M. Spencer, and A. H. England, "Analytical solutions for bending and flexure of helically reinforced cylinders," *Int. J. Solids Struct.*, vol. 40, no. 4, pp. 777–806, 2003.

[9] R. B. Pipes, and P. Hubert, "Helical carbon nanotube arrays: thermal expansion," *Composites Sci. Techn*, vol. 63, no. 11, pp. 1571–1579, 2003.

[10] N. Karathanasopoulos, J.-F. Ganghoffer, and K. O. Papailiou, "Analytical closed-form expressions for the structural response of helical constructions to thermal loads," *Int. J. Mech. Sci.*, vol. 117, pp. 258–264, 2016.

[11] D. Ieşan, "Thermal effects in chiral elastic rods," *Int. J. Therm. Sci.*, vol. 49, no. 9, pp. 1593–1599, 2010.

[12] D. Ieşan, "Thermoelastic deformation of reinforced chiral cylinders," *Acta Mech.*, vol. 228, no. 11, pp. 3901–3922, 2017.

[13] H. Deresiewicz, "Plane waves in a thermoelastic solid," *J. Acoust. Soc. Am.*, vol. 29, no. 2, pp. 204–209, 1957.

[14] B. A. Boley, and I. S. Tolins, "Transient coupled thermoelastic boundary value problems in the half-space," *J. Appl. Mech.*, vol. 29, no. 4, pp. 637–646, 1962.

[15] J. Sharma, D. Singh, and R. Kumar, "Generalized thermoelastic waves in homogeneous isotropic plates," *J. Acoust. Soc. Am.*, vol. 108, no. 2, pp. 848–851, 2000.

[16] H. Singh, and J. N. Sharma, "Generalized thermoelastic waves in transversely isotropic media," *J. Acoust. Soc. Am.*, vol. 77, no. 3, pp. 1046–1053, 1985.

[17] K. Verma, "On the propagation of waves in layered anisotropic media in generalized thermoelasticity," *Int. J. Eng. Sci.*, vol. 40, no. 18, pp. 2077–2096, 2002.

[18] J. Ignaczak, and M. Ostoja-Starzewski, 2010. *Thermoelasticity with Finite Wave Speeds*. Oxford: Oxford University Press. .

[19] H. W. Lord, and Y. Shulman, "A generalized dynamical theory of thermoelasticity," *J. Mech. Phys. Solids*, vol. 15, no. 5, pp. 299–309, 1967.

[20] S. Tomar, and A. Khurana, "Wave propagation in thermo-chiral elastic medium," *Appl. Math. Model.*, vol. 37, no. 22, pp. 9409–9418, 2013.

[21] M. Ostoja-Starzewski, "Thermoelastic waves in a helix with parabolic or hyperbolic heat conduction," *J. Therm. Stresses*, vol. 26, no. 11–12, pp. 1205–1219, 2003.

[22] L. Le Marrec, D. Zhang, and M. Ostoja-Starzewski, "Three-dimensional vibrations of a helically wound cable modeled as a Timoshenko rod," *Acta Mech.*, vol. 229, no. 2, pp. 677–695, 2018.

[23] D. Zhang, and M. Ostoja-Starzewski, "Finite element solutions to the bending stiffness of a single-layered helically wound cable with internal friction," *J. Appl. Mech.*, vol. 83, no. 3, pp. 031003, 2016.

[24] F. Blouin, and A. Cardou, "A study of helically reinforced cylinders under axially symmetric loads and application to strand mathematical modelling," *Int. J. Solids Struct.*, vol. 25, no. 2, pp. 189–200, 1989.

[25] G. A. Costello, 1997. *Theory of Wire Rope*. New York: Springer Science & Business Media.

[26] S. Sathikh, S. Rajasekaran, C. V. Jayakumar, and C. Jebaraj. "General thin rod model for preslip bending response of strand," *J. Eng. Mech.*, vol. 126, no. 2, pp. 132–139, 2000.

[27] H. Shahsavari, and M. Ostoja-Starzewski, "On elastic and viscoelastic helices," *Philos. Mag.*, vol. 85, no. 33-35, pp. 4213–4230, 2005.

[28] L. Xiang, H. Y. Wang, Y. Chen, Y. J. Guan, Y. L. Wang, and L. H. Dai, "Modeling of multi-strand wire ropes subjected to axial tension and torsion loads," *Int. J. Solids Struct*., vol. 58, pp. 233–246, 2015.
[29] M. Raoof, and R. E. Hobbs, "Analysis of multilayered structural strands," *J. Eng. Mech*., vol. 114, no. 7, pp. 1166–1182, 1988.
[30] D. H. Hodges, 2006. *Nonlinear Composite Beam Theory.* Reston: American Institute of Aeronautics and Astronautics, Inc.
[31] D. Hodges, and W. Yu, "A rigorous, engineer-friendly approach for modelling realistic, composite rotor blades," *Wind Energy*, vol. 10, no. 2, pp. 179–193, 2007.
[32] Spencer, A. J. M., 1984, *Continuum Theory of the Mechanics of Fibre-Reinforced Composites*. Vienna: Springer.
[33] L. Rakotomanana, 2009. *Éléments de Dynamique Des Solides et Structures Déformables*. Lausanne, Switzerland: Presses Polytechniques et Universitaires Romandes.
[34] S. Sathikh, M. B. K. Moorthy, and M. Krishnan, "A symmetric linear elastic model for helical wire strands under axisymmetric loads," *J. Strain Anal. Eng. Des*., vol. 31, no. 5, pp. 389–399, 1996.
[35] K. G. McConnell, and W. P. Zemke, "A model to predict the coupled axial torsion properties of ACSR electrical conductors," *Exp. Mech*., vol. 22, no. 7, pp. 237–244, 1982.
[36] H. Ziegler, and C. Wehrli, "The derivation of constitutive relations from the free energy and the dissipation function," *Adv. Appl. Mech.*, vol. 25, pp. 183–238, 1987.
[37] D. R. Bland, 1988. *Wave Theory and Applications*. Oxford: Clarendon Press.
[38] M. Ostoja-Starzewski, 2007. *Microstructural Randomness and Scaling in Mechanics of Materials*. Boca Raton: CRC Press.
[39] J. N. Sharma, and H. Singh, "Generalized thermoelastic waves in anisotropic media," *J. Acoust. Soc. Am.*, vol. 85, no. 4, pp. 1407–1413, 1989.
[40] A. Alawar, E. J. Bosze, S. R. Nutt, "A composite core conductor for low sag at high temperatures," *IEEE Trans. Power Del.*, vol. 20, no. 3, pp. 2193–2199, 2005.
[41] J. Achenbach, 1975. *Wave Propagation in Elastic Solids*. Amsterdam: Elsevier.